On the General Analysis of Coordinated Regularized Zero-Forcing Precoding: An Application to Two-Tier Small-Cell Networks

Harsh Tataria, *Student Member, IEEE*, Peter J. Smith, *Fellow, IEEE*, and Pawel A. Dmochowski, *Senior Member, IEEE*

***Abstract*— General analysis of expected per-terminal signal-to-interference-plus-noise-ratio (SINR) and ergodic per-cell sum spectral efficiency for a multi-cellular system with coordinated regularized zero-forcing (RZF) precoding is presented. An application to two-tier small-cell networks is considered, assuming independent and identically distributed (i.i.d.) and semi-correlated Rayleigh fading channels, with spatial correlation at the base station. Our analysis caters for equal and unequal correlation matrices for each terminal. For the i.i.d. case and when each terminal is assigned an equal correlation matrix, our expressions are averaged over the eigenvalue densities of the channel correlation matrices, which follow an uncorrelated and correlated complex central Wishart distribution. With unequal correlation matrices, we exploit the high signal-to-noise-ratio (SNR) convergence of RZF precoding to zero-forcing (ZF) precoding and use a second-order Neumann series expansion to derive closed-form approximations to the expected RZF SINR and ergodic sum spectral efficiency, via the expected ZF SNR and ergodic sum spectral efficiency. Our numerical results show the adverse effects of intercellular interference, along with the improvements in the above-mentioned performance metrics with network-wide coordination over cell-wide and macro-only coordination strategies. The derived expressions are robust to changes in system dimensions, operating SNRs, and correlation levels.**

***Index Terms*— SINR, spectral efficiency, BS coordination, RZF precoding, two-tier small-cell networks, complex Wishart matrices.**

I. Introduction

MULTIUSER multiple-input multiple-output (MU-MIMO) systems have gained a tremendous amount of attention due to the multiplexing gains resulting from their ability to jointly serve a multiplicity of non-cooperative terminals in the same time-frequency interval [1]. On the downlink, this has led to improvements in the spectral efficiency and bit error rates [2]. However, further challenges arise in practical cellular networks, where downlink transmission takes place simultaneously to terminals in multiple co-channel cells, due to a frequency re-use factor of one. In such systems, due to the increased numbers of interfering sources, inter-cellular interference (ICI) remains an impairment, limiting the achievable performance [3]. As a result, the terminal signal-to-interference-plus-noise-ratio (SINR) can not be improved by simply increasing the base station (BS) transmit power, since this leads to stronger ICI. This is particularly disadvantageous for terminals near the cell-edge, which suffer from lower SINR and spectral efficiency [4].

To minimize such performance loss, BS coordination has been proposed (see e.g., [3]–[5] and references therein), such that multiple BSs could be connected via low-latency, high bandwidth backhaul links, allowing for the transfer of out-of-cell channel state information (CSI). This results in coordinated downlink transmission of data to terminals in multiple cells, while mitigating or reducing intra-cellular interference (IUI) and ICI. Advances in coordinated beamforming have also been made in small-cell networks, as shown in [6] and [7]. Here, different tiers of low powered BSs may operate on the same frequency band as the macrocell, in which case ICI rapidly degrades the terminal SINR with increasing numbers of small-cells [8]. For conventional multi-cellular systems, coordinated beamforming has been extensively studied to evaluate the performance of frequency-division-duplex systems (see [9], [10] and the references therein).

For downlink MU-MIMO systems, linear processing techniques such as matched-filter and zero-forcing (ZF) precoding have been identified as practical alternatives to the optimal, high complexity non-linear approaches, such as dirty-paper-coding [1], [11]. It is well known that in the low signal-to-noise-ratio (SNR) regime, ZF precoding suffers from noise inflation, leading to lower per-terminal spectral efficiency. To compensate for this, regularized zero-forcing (RZF) precoding uses a regularization parameter to control the relative effects of noise and remaining interference at the terminal [12]. RZF has thus proven to be an effective precoding technique for single-cell MU-MIMO systems [13], [14]. Its performance has also been evaluated for multi-cellular systems with large antenna arrays, under independent and identically distributed (i.i.d.), as well as semi-correlated Rayleigh fading channels [15], [16].

The instantaneous distribution of SINR and sum spectral efficiency has also been characterized with stochastic geometry

Manuscript received September 30, 2016; revised February 19, 2017; accepted April 4, 2017. Date of publication April 18, 2017; date of current version July 13, 2017. This paper was presented in part at the International Conference on Communication, Kuala Lumpur, Malaysia, May 2016. The associate editor coordinating the review of this paper and approving it for publication was H.-C. Yang. *(Corresponding author: Harsh Tataria.)*

H. Tataria is with the School of Engineering and Computer Science, Victoria University of Wellington, Wellington 6140, New Zealand, and also with the School of Electronics, Electrical Engineering and Computer Science, Queen's University Belfast, Belfast BT3 9DT, U.K. (e-mail: harsh.tataria@ecs.vuw.ac.nz; h.tataria@qub.ac.uk).

P. J. Smith is with the School of Mathematics and Statistics, Victoria University of Wellington, Wellington 6140, New Zealand (e-mail: peter.smith@vuw.ac.nz).

P. A. Dmochowski is with the School of Engineering and Computer Science, Victoria University of Wellington, Wellington 6140, New Zealand (e-mail: pawel.dmochowski@ecs.vuw.ac.nz).

Color versions of one or more of the figures in this paper are available online at http://ieeexplore.ieee.org.

Digital Object Identifier 10.1109/TCOMM.2017.2695199

often for small-cell networks (see e.g., [17] and references therein). However, the majority of prior work (see [11], [14], [18]–[20]) routinely assumes a fixed spatial correlation matrix for each terminal, despite their geographical differences that lead to different levels of local scattering, in turn resulting in wide variations in the correlation patterns for each terminal [21]. In addition to the inter-element spacing at the BS array, this significantly influences the resulting performance. In the large system regime, deterministic limits to the RZF SINR and sum spectral efficiency with unequal correlation matrices have been analyzed in [13] and [22]. A more general limiting analysis with other types of transmit and receive processing in the presence of unequal correlation structures is presented in [15]. However, in the large system regime, solutions are often presented numerically (see [13], [15], [22]) by iteratively solving a system of fixed point equations, where it is not straightforward to inspect the expressions and evaluate the impact of changes in the system and/or propagation parameters. In contrast to this, we provide explicit analytical expressions that do not require iterative solutions to a set of linked equations. The resulting insights are most obvious in the high SNR regime, where we use ZF precoding to approximate the RZF performance with unequal correlation structures.[1] In general, to derive the expected SINR and expected sum spectral efficiency, we average over the myriad of fast-fading, unless otherwise specified. More specifically, our contributions are as follows:

- We derive tight analytical expressions to approximate the RZF expected per-terminal SINR and ergodic spectral efficiency for i.i.d. and semi-correlated Rayleigh fading channels with spatial correlation at the BS. For equal correlation matrices at each terminal, our expressions are averaged over the arbitrary eigenvalue densities of the instantaneous channel correlation matrix. To the best of our knowledge, such analysis has not been carried out previously and is considered to be cumbersome in [12] and [23], where the expected SINR and ergodic sum spectral efficiencies are averaged over the isotropic eigenvector matrix for simplicity.
- With unequal correlation matrices, we consider the high SNR regime, where RZF precoding converges to ZF precoding. Following the spatial correlation model in [24], we approximate the RZF performance with ZF, and use a second order Neumann series expansion to derive closed-form approximations of the expected ZF SNR and ergodic sum spectral efficiency. In comparison to previous studies, such as [15] and [13], our approximations provide clear insights into the impact of unequal correlation structures, along with other system parameters that influence the achievable expected SNR and ergodic sum spectral efficiency.
- For a two-tier small-cell network, we demonstrate the gain in the expected per-terminal SINR and ergodic spectral efficiencies due to network coordination relative to macro-only and cell-wide coordination. We show the effects of network densification on a per-terminal and system-wide basis with uniform, cell-edge and cell-centric small-cell placement under i.i.d. and semi-correlated fading. The performance of such systems with unequal correlation matrices is superior to that where each terminal is assigned a fixed correlation matrix. We demonstrate the tightness of our approximations with variation in the system dimensions across the SNR range considered.

[1] It is well known that in the high SNR regime, RZF precoding converges to ZF precoding, as the regularization parameter tends to zero (see [12], [14] and references therein).

Notation: We use boldface upper and lower case symbols to represent matrices and vectors. The $M \times M$ identity matrix is denoted as $\boldsymbol{I}_M$, while the (i, j)-th entry of the matrix $\boldsymbol{H}$ is denoted by $\boldsymbol{H}_{i,j}$. The transpose, Hermitian transpose, inverse and trace operators are denoted by $(\cdot)^{\mathrm{T}}$, $(\cdot)^{\mathrm{H}}$, $(\cdot)^{-1}$ and $\mathrm{tr}[\cdot]$, respectively. We use $\boldsymbol{h} \sim \mathcal{CN}\left(0, \sigma^2\right)$ to denote an i.i.d. random vector having complex Gaussian entries with zero mean and variance σ^2. $||\cdot||_{\mathrm{F}}$ and $|\cdot|$ denote the Frobenius and scalar norms, while $\det(\cdot)$, $\mathrm{per}(\cdot)$ and $\lfloor\cdot\rfloor$ denote the determinant, sign of a permutation and floor operators, respectively. $\mathbb{E}[\cdot]$ denotes the statistical expectation over fast-fading, while wherever the expectation is performed over a different random variable, separate notation is introduced in the text. $(\boldsymbol{H})_{\cdot;k}$, $(\boldsymbol{H})_{i;k}$ and $(\boldsymbol{H})_{ij;kl}$ denote the matrix $\boldsymbol{H}$ with column k, row i and column k, as well as rows i, j and columns k, l removed, respectively.

II. Mathematical Preliminaries

A. Channel Models and Eigenvalue Densities

Consider a point-to-point Rayleigh fading MIMO system with M transmit and L receive antennas, respectively. The $L \times M$ channel matrix, $\boldsymbol{H}$, has zero-mean complex Gaussian entries. The statistical properties of such channels rely on the instantaneous channel correlation matrix

$$\boldsymbol{W} \triangleq \begin{cases} \boldsymbol{H}\boldsymbol{H}^{\mathrm{H}} & \text{if } L \leq M \\ \boldsymbol{H}^{\mathrm{H}}\boldsymbol{H} & \text{if } L > M, \end{cases} \tag{1}$$

which follows a complex Wishart distribution. We note that in all cases, $\boldsymbol{H}$ is normalized such that $\mathbb{E}[|\boldsymbol{H}_{i,j}|^2] = 1$. We denote $m = \min(M, L)$ and $n = \max(M, L)$.

Definition 1 (Uncorrelated Rayleigh Fading): Uncorrelated Rayleigh fading is a reasonable model when there is adequate spacing between transmit and receive antenna elements with large angular spreads to induce independent and identically distributed (i.i.d.) fading in $\boldsymbol{H}$. Under these conditions, $\boldsymbol{W}$ follows an uncorrelated complex central Wishart structure with m degrees of freedom (d.o.f.) and a covariance matrix $\boldsymbol{I}_m$. Let λ denote an arbitrary eigenvalue of $\boldsymbol{W}$ drawn from $\lambda_1, \ldots, \lambda_m$. The density of λ, denoted by f_0, is then given in [25]

$$f_0(\lambda) = m^{-1} \sum_{i=1}^{m} \frac{(i-1)}{(i-1+n-m)} \lambda^{n-m} e^{-\lambda} \kappa_{i-1}^{(n-m)}(\lambda)^2, \tag{2}$$

where $\kappa_{i-1}^{(n-m)}$ is a generalized Laguerre polynomial of order $i-1$, defined as

$$\kappa_{i-1}^{(n-m)}(\lambda) \triangleq \sum_{s=0}^{i-1} (-1)^s \binom{i+1+n-m}{i-1-s} \frac{\lambda^s}{s!}. \tag{3}$$

Similarly, let (λ_1, λ_2) be any two arbitrary unordered eigenvalues of $\boldsymbol{W}$. The joint density of such pair is denoted by $f_0(\lambda_1, \lambda_2)$ and is given in [25]

$$f_0(\lambda_1,\lambda_2) = (m(m-1))^{-1} \sum_{i=1}^{m}\sum_{\substack{j=1\\ j\neq i}}^{m} (\lambda_1\lambda_2)^{n-m} e^{-(\lambda_1+\lambda_2)} \times \Phi\left(\kappa_{i-1}^{(n-m)}(\lambda_1)^2 \kappa_{j-1}^{(n-m)}(\lambda_2)^2 - \kappa_{i-1}^{(n-m)}(\lambda_1) \times \kappa_{j-1}^{(n-m)}(\lambda_1)\kappa_{i-1}^{(n-m)}(\lambda_2)\kappa_{j-1}^{(n-m)}(\lambda_2)\right), \tag{4}$$

where

$$\Phi = \frac{(i-1)!\,(j-1)!}{(i-1+n-m)!\,(j-1+n-m)!}. \tag{5}$$

Definition 2 (Semi-Correlated Rayleigh Fading): Due to space limitations in practical MIMO antenna arrays and limited angular spreads, MIMO channels in practice often exhibit a spatially correlated structure. We model the effects of transmit spatial correlation as [26]

$$\boldsymbol{H}_{\mathrm{sc}} = \boldsymbol{H}_{\mathrm{iid}} \boldsymbol{R}_{\mathrm{t}}^{\frac{1}{2}}, \tag{6}$$

where $\boldsymbol{H}_{\mathrm{iid}} \sim \mathcal{CN}(0,1)$ and $\boldsymbol{R}_{\mathrm{t}}$ is a $M \times M$ transmit spatial correlation matrix with M distinct eigenvalues, $\theta_1, \ldots, \theta_M$. Here, $\boldsymbol{W}$ is known to follow a correlated complex central Wishart structure with m d.o.f. and covariance matrix $\boldsymbol{R}_{\mathrm{t}}$. From [27], the density of an arbitrary eigenvalue, λ_{sc}, of the correlated central Wishart matrix is given by

$$f_{\mathrm{o,sc}}(\lambda_{\mathrm{sc}}) = \frac{1}{m\prod_{i<j}^{n}(\theta_j-\theta_i)} \sum_{l=1}^{n}\sum_{k=n-m+1}^{n} \lambda_{\mathrm{sc}}^{m+k-n-1} \times e^{-\lambda_{\mathrm{sc}}/\theta_l}\theta_l^{n-m+1}\mathcal{D}_{l,k}/\,\Gamma(m-n+k), \tag{7}$$

with $\mathcal{D}_{l,k}$ is the (l,k)-th co-factor of a $n \times n$ matrix whose (l,k)-th entry is given by θ_l^{k-1}.

Corollary 1: Let $\boldsymbol{W} = \boldsymbol{H}_{\mathrm{sc}}^{\mathrm{H}}\boldsymbol{H}_{\mathrm{sc}}$, where the $L \times M$ $(L > M)$ channel matrix $\boldsymbol{H}_{\mathrm{sc}} = \boldsymbol{H}_{\mathrm{iid}}\boldsymbol{R}_{\mathrm{t}}^{\frac{1}{2}}$, with $\theta_1, \ldots, \theta_m$ denoting the m distinct eigenvalues of $\boldsymbol{R}_{\mathrm{t}} \neq \boldsymbol{I}_m$. The joint density of any two (unordered) arbitrary eigenvalues of $\boldsymbol{W}$, (λ_1, λ_2), is given by

$$f_{\mathrm{o,sc}}(\lambda_1,\lambda_2) = \hat{\chi}\sum_{i=0}^{m-1}\sum_{\substack{j=0\\ j\neq i}}^{m-1}(-1)^{i+j-p(i,j)}\lambda_1^{i+n-m}\lambda_2^{j+n-m} \times \sum_{k=1}^{m}\sum_{\substack{l=1\\ l\neq k}}^{m}(-1)^{k-1}e^{-\lambda_1/\theta_k}(-1)^{l-p(l)}e^{-\lambda_2/\theta_l} \times \det(\boldsymbol{\Xi})_{i,j;k,l}, \tag{8}$$

where the (l,k)-th element of $\boldsymbol{\Xi}$ is given by $e^{-\lambda_l}/\theta_k$ and $\hat{\chi} = \chi(-1)^{\lfloor \frac{m}{2} \rfloor}(m-2)!$ with

$$\chi = \frac{1}{m!\prod_{l=1}^{m}(n-l)!\det(\boldsymbol{R}_{\mathrm{t}})^n \prod_{k<l}^{m}\left(\frac{1}{\theta_l}-\frac{1}{\theta_k}\right)}. \tag{9}$$

Moreover,

$$p(i,j) = \begin{cases} 0 & \text{if } i > j \\ 1 & \text{if } i \leq j \end{cases} \text{ and } p(l) = \begin{cases} 0 & \text{if } k > l \\ 1 & \text{if } k \leq l. \end{cases} \tag{10}$$

Proof: The joint density of L unordered eigenvalues is given in matrix tensor form in [28]. From the result in [28], the density can be expressed in terms of determinants which are then expanded via Laplace expansions of the columns containing λ_1 and λ_2 to give (8). ■

Corollary 2: Let $\boldsymbol{W} = \boldsymbol{H}_{\mathrm{sc}}\boldsymbol{H}_{\mathrm{sc}}^{\mathrm{H}}$, where the $L \times M$ $(M \geq L)$ channel matrix $\boldsymbol{H}_{\mathrm{sc}} = \boldsymbol{H}_{\mathrm{iid}}\boldsymbol{R}_{\mathrm{t}}^{\frac{1}{2}}$, with $\theta_1, \ldots, \theta_n$ denoting the n distinct eigenvalues of $\boldsymbol{R}_{\mathrm{t}} \neq \boldsymbol{I}_n$. The joint density of any two (unordered) arbitrary eigenvalues of $\boldsymbol{W}$, (λ_1, λ_2), is given by

$$f_{\mathrm{o,sc}}(\lambda_1,\lambda_2) = T(n-2)!\sum_{i=0}^{m-1}\sum_{\substack{j=0\\ j\neq i}}^{m-1}(-1)^{i+1-p(i,l)}\sum_{o=1}^{m}(-1)^{o-1} \times \theta_o^{n-m-1}\lambda_1^i e^{-\lambda_1/\theta_0}\sum_{\substack{p=1\\ p\neq o}}^{m}(-1)^{p-p(o)}\theta_p^{n-m-1} \times \lambda_2^j e^{-\lambda_2/\theta_p}\boldsymbol{\Theta}, \tag{11}$$

where $T = 1/\prod_{j=1}^{n} j!\det(\boldsymbol{\Delta}_n)$, with $\boldsymbol{\Delta}_n$ defined as the $n \times n$ Vandermonde matrix

$$\boldsymbol{\Delta}_n \triangleq \begin{bmatrix} 1 & \theta_1 & \ldots & \theta_1^{n-1} \\ \vdots & \vdots & \ddots & \vdots \\ 1 & \theta_n & \ldots & \theta_n^{n-1} \end{bmatrix}, \tag{12}$$

$p(i,l)$ and $p(o)$ are equivalently defined in (10), while $\boldsymbol{\Theta} \triangleq \det\left(\left(\boldsymbol{\Delta}_{n,m}\right)_{o,p;i+n-m+1,j+n-m+1}\right)$ with

$$\boldsymbol{\Delta}_{n,m} \triangleq \begin{bmatrix} 1 & \ldots & \theta_1^{n-m-1} & \theta_1^{n-m-1}e^{-\lambda_1/\theta_1} & \ldots \\ \vdots & \vdots & \vdots & \vdots & \vdots \\ 1 & \ldots & \theta_n^{n-m-1} & \theta_n^{n-m-1}e^{-\lambda_1/\theta_n} & \ldots \end{bmatrix}. \tag{13}$$

Proof: Following the procedure in Appendix A with Corollary 1 yields the desired result. ■

Remark 1: We note that the results in Corollaries 1 and 2 have been derived by Zanella and Chiani [28] in tensor form. This form can also be used here, however, for the ease of subsequent analysis, we expand these densities into finite summations resulting in (8) and (11), respectively.

B. Integrals and Special Functions

Throughout the paper, we make use of the following integrals and special functions. Let

$$J_{a,b,c}(\xi) = \int_0^{\infty} \frac{\lambda^a e^{-\lambda/c}}{(\lambda+\xi)^b} d\lambda, \quad \text{where } a, b \text{ and } c \geq 1. \tag{14}$$

We solve (14) by substituting $\lambda = \omega - \xi$ to obtain

$$J_{a,b,c}(\xi) = \int_{\xi}^{\infty} \frac{(\omega-\xi)^a e^{-(\omega-\xi)/c}}{\omega^b} d\omega = \sum_{f=0}^{a}\binom{a}{f}(-\xi)^{a-f}e^{\xi/c}\underbrace{\int_{\xi}^{\infty}\omega^{f-b}e^{-\omega}d\omega}_{J^{(b)}}. \tag{15}$$

We are interested in two special cases of $J^{(b)}(\xi)$, when $b = 1$ and $b = 2$. These are given by

$$J^{(1)}(\xi) = \int_{\xi}^{\infty} \omega^{f-1} e^{-\omega} d\omega = \begin{cases} \mathrm{Ei}(1,\xi) & \text{if } f = 0 \\ \Gamma(f,\xi) & \text{if } f \geq 1, \end{cases} \quad (16)$$

and

$$J^{(2)}(\xi) = \int_{\xi}^{\infty} \omega^{f-2} e^{-\omega} d\omega = \begin{cases} -\mathrm{Ei}(1,\xi) + \frac{e^{-\xi}}{\xi^2} & \text{if } f = 0 \\ \mathrm{Ei}(1,\xi) & \text{if } f = 1 \\ \Gamma(f-1,\xi) & \text{if } f \geq 2, \end{cases} \quad (17)$$

where $\mathrm{Ei}(\cdot,\cdot)$ is the generalized exponential integral and $\Gamma(\cdot,\cdot)$ is the incomplete gamma function.

III. System Model

A. Downlink Received Signal

We consider the downlink of a two-tier, multi-cellular, MU-MIMO system with K cells in total, where tier one consists of macro and tier two consists of microcell BSs. BS k, located at the origin of cell k in either tier is equipped with M_k transmit antennas, simultaneously serving L_k non-cooperative single antenna user terminals in the same time-frequency interval. We assume that perfect backhaul links with zero latency and infinite bandwidth are present between the K cells. We also assume narrow-band transmission with uniform power allocation. We denote the $1 \times M_k$ downlink channel vector from BS k to terminal l located in cell k as $\boldsymbol{h}_{k,l,k}$. The ICI channel from BS j to user terminal l in cell k is denoted by $\boldsymbol{h}_{j,l,k}$, where $j \neq k$. Both the desired and interfering channels are assumed to follow correlated Rayleigh fading with $\boldsymbol{h}_{j,l,k} = \boldsymbol{u}_{j,l,k} \boldsymbol{R}_{j,l,k}^{\frac{1}{2}}$, where $\boldsymbol{u}_{j,l,k} \sim \mathcal{CN}(0, \boldsymbol{I}_{M_j})$ and $\boldsymbol{R}_{j,l,k}$ is the transmit spatial correlation matrix for channel $\boldsymbol{h}_{j,l,k}$. In the case where each terminal has an equal correlation matrix, $\boldsymbol{R}_{j,l,k} = \boldsymbol{R}_j$; $\forall l, k$. Whilst we postpone the discussion of the particular structure of $\boldsymbol{R}_{j,l,k}$ to Section VI, we note the generality of the presented channel model, allowing us to consider any type of antenna correlation structure in $\boldsymbol{R}_{j,l,k}$. Although we consider the general case of MU-MIMO in a two-tier small-cell network, the above model is also of relevance to large antenna arrays, where strong antenna correlation may arise due to inadequate inter-element spacing or lack of multi-path diversity [15].

With CSI at BS k, the received signal at the l-th terminal in the k-th cell is given by

$$y_{l,k} = \underbrace{\sqrt{\frac{\beta_{k,l,k}}{\eta_k}} \boldsymbol{h}_{k,l,k} \boldsymbol{g}_{l,k} s_{l,k}}_{\text{desired signal}} + \underbrace{\sqrt{\frac{\beta_{k,l,k}}{\eta_k}} \sum_{\substack{m=1 \\ m \neq l}}^{L_k} \boldsymbol{h}_{k,l,k} \boldsymbol{g}_{m,k} s_{m,k}}_{\text{intra-cellular interference (IUI)}} + \underbrace{\sum_{\substack{j=1 \\ j \neq k}}^{K} \sqrt{\frac{\beta_{j,l,k}}{\eta_j}} \boldsymbol{h}_{j,l,k} \sum_{q=1}^{L_j} \boldsymbol{g}_{q,j} s_{q,j}}_{\text{inter-cellular interference (ICI)}} + \underbrace{\bar{v}_l}_{\text{noise}}, \quad (18)$$

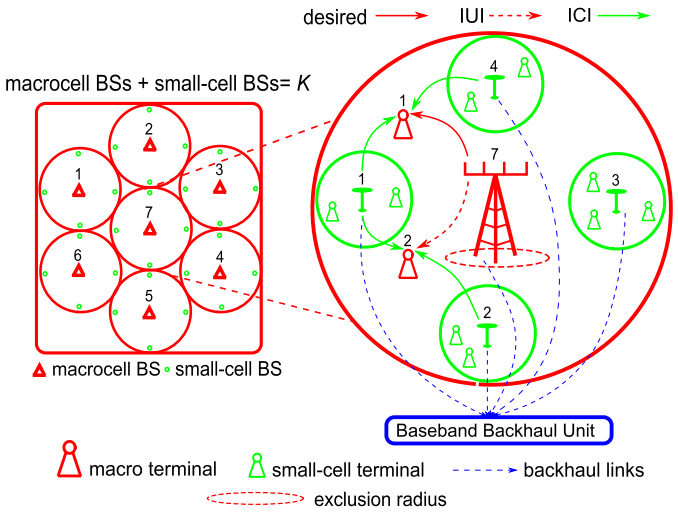

Fig. 1. Two-tier small-cell network with randomly distributed small-cells in each macrocell.

where $\boldsymbol{g}_{l,k}$ is the $M_k \times 1$ un-normalized precoding vector for the l-th terminal in cell k and η_k is the precoder normalization parameter, discussed later, for the k-th cell. $s_{l,k}$ is the transmitted data symbol from BS k to terminal l with unit mean power and $\bar{v}_l$ denotes white Gaussian noise at the l-terminal where $\bar{v}_l \sim \mathcal{CN}(0, \sigma_l^2)$. $\beta_{k,l,k}$ and $\beta_{j,l,k}$ are the desired and interfering received powers at the l-th terminal in cell k from the desired and interfering BSs, respectively. We model the received power from BS j to terminal l in cell k as [29]

$$\beta_{j,l,k} = P_{\mathrm{t},j} \varsigma \left(\frac{d_0}{d_{j,l,k}} \right)^{\alpha_j} \psi_{j,l,k}. \quad (19)$$

Here, $P_{\mathrm{t},j}$ is the transmit power of BS j. Note that the transmit power of a given BS depends on the tier it is located in. ς is a unit-less constant for geometric attenuation at the reference distance d_0, assuming far-field, omni-directional transmit antennas. $d_{j,l,k}$ is the distance from BS j to terminal l in cell k and α_j is the attenuation exponent dependent on the transmitting BS and the propagation scenario. $\psi_{j,l,k} = 10^{(S\sigma_s/10)}$ models the effects of shadow-fading with a log-normal distribution, where $S \sim \mathcal{N}(0,1)$ and σ_s is the shadow-fading standard deviation. Fig. 1 depicts a typical two-tier network configuration composed of multiple macro and overlaid small-cells. We show the effects of downlink propagation to terminal 1 in macrocell 7's coverage area, as it causes IUI to terminal 2 and experiences ICI from the nearby micro BSs. Each BS is connected via the baseband backhaul unit and K is the total number of BSs in the network (macro and small-cell). For adequate quality of service provisioning, we include an exclusion radius around the macro BS, where no small-cells can be located.

B. Transmit Spatial Correlation Scenarios

The literature contains many studies where correlation matrices are assumed equal for each terminal [11], [14], [18]–[20] as well as studies considering unequal correlation matrices [13], [15], [22], [24], [30]. In situations where the BS illuminates the same set of scatterers for all terminals, a constant transmit correlation matrix is valid. For example,

if the BS is surrounded by a ring of scatterers, then the resultant correlation matrices are simply governed by a zeroth-order Bessel function of the first kind. Naturally, this is a more sensible model at the terminal, which may be in dense clutter. Nevertheless, it illustrates the point that when the departing rays from the BS arrive at the same scatterers, then constant correlation matrices occur. In contrast to this, the model in [30] essentially assumes that the BS illuminates separate rings of scatterers around each terminal. This gives rise to wide variations in the correlations for different terminals. These are extreme cases where the BS illuminates either the same or disjoint sets of scatterers for each terminal. In reality, it is likely that some scatterers are common to some terminals and distinct to others. This is an interesting modeling question outside the scope of this paper. Here we focus on the two edge cases of equal and unequal correlation matrices using the models in [24].

C. Regularized Zero-Forcing (RZF) Precoding

We consider RZF precoding [12] to design the downlink beamforming vectors to each terminal. First, we focus on the case where each BS performs RZF to terminals in its own coverage area, and later we extend this to other network coordination types. The un-normalized RZF precoding vector for the l-th terminal in cell k is the l-th column of the $M_k \times L_k$ matrix, $\boldsymbol{G}_k$, such that

$$\boldsymbol{G}_k \triangleq \boldsymbol{H}_k^{\mathrm{H}} \left(\boldsymbol{H}_k \boldsymbol{H}_k^{\mathrm{H}} + \xi_k \boldsymbol{I}_{L_k} \right)^{-1}, \tag{20}$$

where $\boldsymbol{H}_k \triangleq [\boldsymbol{h}_{k,1,k}^{\mathrm{T}}, \boldsymbol{h}_{k,2,k}^{\mathrm{T}}, \ldots, \boldsymbol{h}_{k,L_k,k}^{\mathrm{T}}]^{\mathrm{T}}$ is the composite matrix containing the channel vectors of all L_k terminals in cell k. Following [31], we normalize the precoder matrix in (20) by $\eta_k = ||\boldsymbol{G}_k||^2 / L_k$ ensuring $\mathbb{E}\left[||\boldsymbol{g}_{l,k}||^2\right] = 1$. The constant $\xi_k > 0$ denotes the regularization parameter designed at BS k. Following [31], we consider

$$\xi_k = \frac{1}{KL} \sum_{k=1}^{K} \sum_{\substack{l=1 \\ l \neq k}}^{L_k} \frac{1}{\beta_{k,l,k}}, \tag{21}$$

where K and L are the total number of cells and terminals within the system, respectively. While selecting ξ_k to maximize the SINR has been considered in [12] for a single-cell system, maximization of SINR in the case of multiple cells leads to a coupled optimization problem [12]. The computation of ξ_k in (21) requires BS k to know all large-scale fading coefficients, and assumes ideal backhaul links to deliver the large-scale fading parameters of all terminals to BS k. This assumption is reasonable, since RZF requires CSI at the BS and large-scale fading co-efficients vary much more slowly than the fast-fading.

D. Network Coordination Strategies

1) Cell-Wide Coordination: In this strategy, the BSs in both tiers perform single-cell RZF processing. That is, each BS coordinates the desired and IUI locally. ICI is, however, present from other cells, as the RZF precoder does not consider any ICI channels in its design. The composite channel matrix to compute the RZF precoders for L_k terminals in cell k is given by

$$\boldsymbol{H}_k \triangleq \left[\boldsymbol{h}_{k,1,k}^{\mathrm{T}}, \boldsymbol{h}_{k,2,k}^{\mathrm{T}}, \ldots, \boldsymbol{h}_{k,L_k,k}^{\mathrm{T}} \right]^{\mathrm{T}}. \tag{22}$$

2) Network-Wide Coordination: In this strategy, the serving BS applies RZF precoding not only to the channels of its own terminals, but also considers ICI to other terminals in the system. The serving and interfering links can be determined using cell-specific pilot signaling (assuming perfect channel estimation in the absence of pilot contamination and the availability of sufficient number of orthogonal reference signals). Then, all interfering channels from other cells are delivered to the serving cell BS via the backhaul interface. The composite channel matrix, $\boldsymbol{H}_k$, for cell k with network-wide coordinated RZF processing can now be defined as

$$\boldsymbol{H}_k \triangleq \left[\boldsymbol{Z}_1^{\mathrm{T}}, \boldsymbol{Z}_2^{\mathrm{T}}, \ldots, \boldsymbol{Z}_j^{\mathrm{T}}, \ldots, \boldsymbol{Z}_K^{\mathrm{T}} \right]^{\mathrm{T}}, \tag{23}$$

where $\boldsymbol{Z}_j \triangleq \left[\boldsymbol{h}_{j,1,k}^{\mathrm{T}}, \ldots, \boldsymbol{h}_{j,L_k,k}^{\mathrm{T}} \right]^{\mathrm{T}}$. With this composite channel matrix, (20) can still be used, however, the precoder $\boldsymbol{G}_k$ only contains the L_k columns of (20) corresponding to the terminals in cell k (columns $\sum_{i=1}^{k-1} L_i + 1$ to $\sum_{i=1}^{k} L_i$). Similarly, η_k is the Frobenius norm of $\boldsymbol{G}_k$ with L_k columns only. Since network-wide coordination requires knowledge of all instantaneous channel vectors at BS k, it introduces significant backhaul overheads. Whilst not practical, such a strategy allows us to evaluate the upper bound (best case performance) of the expected per-terminal SINR and ergodic per-cell spectral efficiency in such interference dominated scenarios.

3) Macro-Only Coordination: In this strategy, we assume that the macrocell BSs have knowledge of the ICI channels to terminals located in tier-two cells. The macrocells then utilize this out-of-cell CSI to coordinate downlink transmission to its own, as well as to terminals in tier-two cells. The composite channel used to obtain the RZF precoding matrix for BS k is equivalent to (23) and (22), if BS k is a macro and microcell, respectively.

IV. Expected Per-Terminal SINR and Ergodic Per-Cell Spectral Efficiency

From (18), the SINR at the l-th terminal in cell k being served by BS k can be written as

$$\rho_{l,k} = \frac{\frac{\beta_{k,l,k}}{\eta_k} |\boldsymbol{h}_{k,l,k} \boldsymbol{g}_{l,k}|^2}{\sigma_l^2 + \frac{\beta_{k,l,k}}{\eta_k} \sum\limits_{\substack{m=1 \\ m \neq l}}^{L_k} |\boldsymbol{h}_{k,l,k} \boldsymbol{g}_{m,k}|^2 + \sum\limits_{\substack{j=1 \\ j \neq k}}^{K} \frac{\beta_{j,l,k}}{\eta_j} \sum\limits_{q=1}^{L_j} |\boldsymbol{h}_{j,l,k} \boldsymbol{g}_{q,j}|^2}. \tag{24}$$

From (24), the expected per-terminal SINR can be obtained by performing $\mathbb{E}\left[\rho_{l,k}\right]$. Exact evaluation of $\mathbb{E}\left[\rho_{l,k}\right]$ is cumbersome, thus we employ the commonly used first-order delta method expansion as shown in [14], [32], and [32]–[34] to

approximate $\mathbb{E}\left[\rho_{l,k}\right]$, allowing us to write

$$\mathbb{E}\left[\rho_{l,k}\right] \approx \frac{\frac{\beta_{k,l,k}}{\tilde{\eta}_k}\mathbb{E}\left[|\boldsymbol{h}_{k,l,k}\boldsymbol{g}_{l,k}|^2\right]}{\sigma_l^2+\frac{\beta_{k,l,k}}{\tilde{\eta}_k}\sum\limits_{\substack{m=1\\m\neq l}}^{L_k}\mathbb{E}\left[|\boldsymbol{h}_{k,l,k}\boldsymbol{g}_{m,k}|^2\right]+\sum\limits_{\substack{j=1\\j\neq k}}^{K}\frac{\beta_{j,l,k}}{\tilde{\eta}_j}\sum\limits_{q=1}^{L_j}\mathbb{E}\left[|\boldsymbol{h}_{j,l,k}\boldsymbol{g}_{q,j}|^2\right]}, \tag{25}$$

where the quantities $\tilde{\eta}_k \triangleq \mathbb{E}[\eta_k]$ and $\tilde{\eta}_j \triangleq \mathbb{E}\left[\eta_j\right]$, respectively.

Remark 2: The approximation used in (25) is a standard first-order Delta expansion and is of the form $\mathbb{E}\left[\frac{X}{Y}\right] \approx \frac{\mathbb{E}[X]}{\mathbb{E}[Y]}$, where X and Y contain standard quadratic forms [14], [32], [32], [34], [35]. The accuracy of such approximations relies on Y having a small variance relative to its mean. This can be seen by applying a multivariate Taylor series expansion of $\frac{X}{Y}$ around $\frac{\mathbb{E}[X]}{\mathbb{E}[Y]}$, as shown in the analysis methodology of [34], [35]. In particular, the quadratic forms in (25) are well suited to this approximation as M_k and L_k start to increase, where the approximation is shown to be extremely tight. This is due to the quadratic forms averaging their respective individual components, minimizing their variance relative to their mean. For further discussion, we refer the interested reader to Appendix I of [34], where a detailed mathematical proof of the approximation accuracy can be found.

From (25), the resulting ergodic spectral efficiency for terminal l in cell k (in bits/seconds/Hz) is given by $\mathbb{E}\left[\mathrm{R}_{l,k}\right] = \mathbb{E}\left[\log_2\left(1+\rho_{l,k}\right)\right]$. As such, the ergodic sum spectral efficiency for the L_k terminals in cell k can be approximated as

$$\begin{aligned}\mathbb{E}\left[\mathrm{R}_{\mathrm{sum},k}\right] &= \mathbb{E}\left[\sum_{l=1}^{L_k}\log_2\left(1+\rho_{l,k}\right)\right]\\ &\approx \sum_{l=1}^{L_k}\log_2\left(1+\mathbb{E}\left[\rho_{l,k}\right]\right).\end{aligned} \tag{26}$$

Remark 3: Note that (26) leads to an approximation rather an upper bound via Jensen's inequality, as the value of $\mathbb{E}\left[\rho_{l,k}\right]$ is itself an approximation [36]. Moreover, the summation over L_k terminals in cell k takes care of the fact that $\mathbb{E}\left[\rho_{l,k}\right]$ could be different depending on l and k, due to relative differences in the physical location of the terminal, causing further differences in the level of geometric attenuation and log-normal shadow-fading.

A. Expected Signal Power

The expected signal power in (25) is given by

$$\delta_{l,k} = \frac{\beta_{k,l,k}}{\tilde{\eta}_k}\mathbb{E}\left[|\boldsymbol{h}_{k,l,k}\boldsymbol{g}_{l,k}|^2\right]. \tag{27}$$

Via an eigenvalue decomposition, we denote $\boldsymbol{H}_k\boldsymbol{H}_k^{\mathrm{H}} = \boldsymbol{U}\boldsymbol{\Lambda}\boldsymbol{U}^{\mathrm{H}}$. The expectation in (27) over the isotropic distribution of $\boldsymbol{U}$ can be written as [12]

$$\varrho_{l,k} = \mathbb{E}\left[|\boldsymbol{h}_{k,l,k}\boldsymbol{g}_{l,k}|^2\right] = \mathbb{E}\left[\left(\sum_{l=1}^{m}\frac{\lambda_l}{\lambda_l+\xi_k}|u_{k,l}|^2\right)^2\right], \tag{28}$$

where m is the minimum of the transmit and receive dimensions. For cell-wide coordination, $m \triangleq \min\left(L_k, M_k\right)$, whilst for network-wide coordination, $m \triangleq \min\left(\sum_{k=1}^{K}L_k, M_k\right)$, respectively. λ_l is the l-th eigenvalue corresponding to the l-th diagonal entry in $\boldsymbol{\Lambda}$ and $u_{k,l}$ denotes the (k,l)-th entry of $\boldsymbol{U}$. (28) can be further averaged over the entries of $\boldsymbol{U}$ and can be written as [12]

$$\begin{aligned}\varrho_{l,k} &= \mathbb{E}\left[|\boldsymbol{h}_{k,l,k}\boldsymbol{g}_{l,k}|^2\right]\\ &= \frac{1}{m\left(m+1\right)}\left\{\mathbb{E}_\lambda\left[\left(\sum_{l=1}^{m}\frac{\lambda_l}{\lambda_l+\xi_k}\right)^2\right]\right.\\ &\qquad\left.+\,\mathbb{E}_\lambda\left[\sum_{l=1}^{m}\left(\frac{\lambda_l}{\lambda_l+\xi_k}\right)^2\right]\right\},\end{aligned} \tag{29}$$

where $\mathbb{E}_\lambda[\cdot]$ denotes the expectation over the eigenvalues. From this, $\tilde{\eta}_k$ can also be inferred as

$$\tilde{\eta}_k = \tau\mathbb{E}\left[||\boldsymbol{G}_k||_{\mathrm{F}}^2\right] = \tau\mathbb{E}_\lambda\left[\sum_{l=1}^{m}\frac{\lambda_l}{\left(\lambda_l+\xi_k\right)^2}\right], \tag{30}$$

where $\tau = \frac{1}{L_k}$ for cell-wide and $\frac{1}{\sum_{k=1}^{K}L_k}$ for network-wide coordination, as every column of $\boldsymbol{G}_k$ is identically distributed. The expressions in (29) and (30) can be further averaged over the density of the eigenvalues as shown in the following Theorems and Lemmas for uncorrelated and semi-correlated Rayleigh fading channels with equal correlation matrices.

Theorem 1: When $\boldsymbol{R}_k = \boldsymbol{I}_m$, the expected value of $\sum_{i=1}^{m}\frac{\lambda_i^\mu}{\left(\lambda_i+\xi_k\right)^2}$, over the eigenvalues of $\boldsymbol{H}_k\boldsymbol{H}_k^{\mathrm{H}}$ is given by

$$\begin{aligned}S_k^\mu = \sum_{i=1}^{m}\frac{(i-1)!}{(i-1+n-m)!}\sum_{z=0}^{i-1}\sum_{\substack{l=0\\l\neq z}}^{i-1}(-1)^{z+l}\binom{i-1+n-m}{i-1-z}\\ \times\binom{i-1+n-m}{i-1-l}\frac{1}{z!l!}J_{\mu+n-m+z-l,2,1}\left(\xi_k\right),\end{aligned} \tag{31}$$

where $J_{\mu+n-m+z-l,2,1}\left(\xi_k\right)$ is as defined in (15).

Proof: See Appendix A. ∎

Theorem 2: For $M_k \leq L_k$ or $M_k > L_k$, where $\theta_1,\ldots,\theta_n$ are the eigenvalues of $\boldsymbol{R}_k \neq \boldsymbol{I}_n$, the expected value of $\sum_{i=1}^{m}\frac{\lambda_i^{\bar{\mu}}}{\left(\lambda_i+\xi_k\right)^2}$, over the eigenvalues of $\boldsymbol{H}_k\boldsymbol{H}_k^{\mathrm{H}}$ is given by

$$\begin{aligned}\bar{S}_k^{\bar{\mu}} = \frac{1}{\prod_{i<j}^{n}\left(\theta_j-\theta_i\right)}\sum_{l=1}^{n}\sum_{k=n-m+1}^{n}\frac{\theta_l^{n-m-1}\mathcal{D}_{l,k}}{\Gamma\left(m-n+k\right)}\\ \times J_{m+k-n-1+\bar{\mu},2,\theta_l}\left(\xi_k\right),\end{aligned} \tag{32}$$

where $\mathcal{D}_{l,k}$ and $J_{m+k-n-1+\bar{\mu},2,\theta_l}\left(\xi_k\right)$ are as defined in (7) and (15), respectively.

Proof: See Appendix B. ∎

Lemma 1: When $\boldsymbol{R}_k = \boldsymbol{I}_m$, the expected value of $\left(\sum_{i=1}^{m} \frac{\lambda_i}{\lambda_i+\xi_k}\right)^2$ is given by

$$Q_k = S_k^2 + \sum_{i=1}^{m}\sum_{\substack{j=1\\ j\neq i}}^{m} \Phi \times \left\{ \left(\sum_{f=0}^{i-1}\sum_{\substack{z=0\\ z\neq f}}^{i-1} (-1)^{f+z} \binom{n-m+i-1}{i-1-f} \times \binom{n-m+i-1}{i-1-z} \frac{1}{f!z!} J_{n-m+1-f+z,1,1}(\xi_k) \right)^2 + \left(\sum_{f=0}^{i-1}\sum_{\substack{z=0\\ z\neq f}}^{i-1} (-1)^{f+z} \binom{n-m+i-1}{i-1-f} \times \binom{n-m+j-1}{i-1-f} \times \frac{1}{f!z!} J_{n-m+1+f+z,1,1}(\xi_k) \right)^2 \right\}, \quad (33)$$

where Φ and $J_{n-m+1+f+z,1,1}(\xi_k)$ are as defined in (5) and (15), respectively.

Proof: See Appendix C. ■

Lemma 2: Let $M_k \leq L_k$, where $\theta_1, \ldots, \theta_m$ are the m eigenvalues of $\boldsymbol{R}_k \neq \boldsymbol{I}_m$. The expected value of $\left(\sum_{i=1}^{m} \frac{\lambda_i}{\lambda_i+\xi_k}\right)^2$ is given by

$$\bar{Q}_k = \bar{S}_k^2 + \hat{\chi} \sum_{i=0}^{m}\sum_{\substack{j=0\\ j\neq i}}^{m}\sum_{k=1}^{m}\sum_{\substack{l=1\\ l\neq k}}^{m} (-1)^{i+j-p(i,j)} (-1)^{k-1+l-p(l)} \times \det(\boldsymbol{\Xi})_{i,j;k,l} J_{i+n-m+1,1,\theta_k}(\xi_k) J_{j+n-m+1,1,\theta_l}(\xi_k), \quad (34)$$

where $\hat{\chi}$, $p(i,j)$, $p(l)$ and $\boldsymbol{\Xi}$ are as defined in (8) and (10), respectively. The integrals $J_{i+n-m+1,1,\theta_k}(\xi_k)$ and $J_{j+n-m+1,1,\theta_l}(\xi_k)$ are defined in (15).

Proof: See Appendix D. ■

Lemma 3: Let $M_k > L_k$, where $\theta_1, \ldots, \theta_n$ are the n eigenvalues of $\boldsymbol{R}_k \neq \boldsymbol{I}_n$. The expected value of $\left(\sum_{i=1}^{m} \frac{\lambda_i}{\lambda_i+\xi_k}\right)^2$ is given by

$$\tilde{Q}_k = \bar{S}_k^2 + n(n-1)\chi(n-2)! \sum_{i=0}^{n-1}\sum_{\substack{l=0\\ l\neq i}}^{n-1}\sum_{o=1}^{n}\sum_{\substack{p=1\\ p\neq o}}^{n} (-1)^{i+1-p(i,l)} \times (-1)^{o-1+p-p(i,l)} (-1)^{o-1+p-p(o)} \theta_o^{n-m-1} \det(\boldsymbol{\Delta}_n)_{o,p} \times \det(\boldsymbol{\Xi})_{i,l;o,p} J_{i+1,1,\theta_o}(\xi_k) J_{l+1,1,\theta_p}(\xi_k). \quad (35)$$

The quantities χ, $p(i,l)$ and $p(o)$ are as given in (9) and (10). Moreover, $\boldsymbol{\Delta}_n$ and $\boldsymbol{\Xi}$ are as defined in (12) and (8), respectively.

Proof: Following the steps in Appendix D using (7) and (11) yields the desired result. ■

Remark 4: The generality of the results derived in Theorems 1, 2 and Lemmas 1, 2 and 3 is worth mentioning. The results are applicable for any system dimension, operating SNR and spatial correlation level. The analysis methodology is also applicable to other channel models (so long as the necessary densities are known), such as i.i.d and semi-correlated Ricean fading. Although we consider an application to two-tier small-cell networks, the results are equally as applicable to classical multi-cellular systems operating with conventional or large antenna arrays.

Remark 5: The results of Lemmas 2 and 3 have further applications to analysis involving complex correlated central Wishart matrices, such as the analysis of second order statistics of semi-correlated channels, leading to the variance of capacity for such channels.

Using the results derived in Theorems 1, 2 and Lemmas 1, 2, 3, we can express (29) for i.i.d. and semi-correlated Rayleigh fading channels as in (36), as shown at the top of the next page. In the same manner, the expected value of the normalization parameter, $\tilde{\eta}_k$ for cell k can also be stated for i.i.d. and semi-correlated Rayleigh fading channels, as in (37). These are shown on top of the next page.

Thus, the expected signal power, $\delta_{l,k}$, in (27) can be written in (38) on top of the next page for the i.i.d. case and semi-correlated cases, respectively.

B. Expected Interference Power

From (25), the expected interference power at the l-th terminal in cell k is given by

$$\iota_{l,k} = \frac{\beta_{k,l,k}}{\tilde{\eta}_k} \left\{ \sum\nolimits_{\substack{m=1\\ m\neq l}}^{L_k} \mathbb{E}\left[|\boldsymbol{h}_{k,l,k} \boldsymbol{g}_{m,k}|^2 \right] \right\} + \sum_{\substack{j=1\\ j\neq k}}^{K} \frac{\beta_{j,l,k}}{\tilde{\eta}_j} \left\{ \sum\nolimits_{q=1}^{L_j} \mathbb{E}\left[|\mathbf{h}_{j,l,k} \boldsymbol{g}_{q,j}|^2 \right] \right\}. \quad (39)$$

For network-wide coordination, following the methodology of [12], the expected interference power can be evaluated as the difference between the total power (signal and interference) and the desired signal power at the l-th terminal in cell k. The total power at terminal l is given by

$$\gamma_{l,k} = \mathbb{E}\left[||\boldsymbol{H}_k \boldsymbol{G}_k||_{\mathrm{F}}^2 \right] = \tau L_k \left\{ \mathbb{E}_\lambda \left[\sum_{l=1}^{m} \left(\frac{\lambda_l}{\lambda_l + \xi_k} \right)^2 \right] \right\}. \quad (40)$$

Subtracting the expected desired signal power in $\delta_{l,k}$ from $\gamma_{l,k}$ yields the interference power at the l-th terminal in cell k. More specifically, under i.i.d. Rayleigh fading, $\iota_{l,k}$ is given by

$$\iota_{l,k}^{\text{i.i.d.}} = \frac{\beta_{k,l,k}}{\tilde{\eta}_k^{\text{i.i.d.}}} \left\{ \left(\frac{L_k - 1}{M_k - 1} \right) \left(\gamma_{l,k}^{\text{i.i.d.}} - \varrho_{l,k}^{\text{i.i.d.}} \right) \right\} + \sum_{\substack{j=1\\ j\neq k}}^{K} \frac{\beta_{j,l,k}}{\tilde{\eta}_j^{\text{i.i.d.}}} \left\{ \left(\frac{L_k}{M_k - 1} \right) \left(\gamma_{l,j}^{\text{i.i.d.}} - \varrho_{l,j}^{\text{i.i.d.}} \right) \right\}. \quad (41)$$

The equivalent expressions for semi-correlated scenarios, $\iota_{l,k}^{M_k \leq L_k}$ and $\iota_{l,k}^{M_k > L_k}$, can be obtained by replacing $\tilde{\eta}_k^{\text{i.i.d.}}$, $\tilde{\eta}_j^{\text{i.i.d.}}$, $\gamma_{l,k}^{\text{i.i.d.}}$, $\gamma_{l,j}^{\text{i.i.d.}}$, $\varrho_{l,k}^{\text{i.i.d.}}$ and $\varrho_{l,j}^{\text{i.i.d.}}$ with their semi-correlated counterparts for $M_k \leq L_k$ and $M_k > L_k$, respectively. With cell-wide coordination, the above approach can be used to find the IUI (first term in (39)). However, as the RZF processor designed at BS k is independent of the ICI channels, the second term

$$\varrho_{l,k}^{\text{i.i.d.}} = \frac{Q_k + S_k^{(2)}}{m\,(m+1)}, \quad \varrho_{l,k}^{\text{s.c.},M_k \le L_k} = \frac{\bar{Q}_k + \bar{S}_k^{(2)}}{m\,(m+1)}, \; \varrho_{l,k}^{\text{s.c.},M_k > L_k} = \frac{\tilde{Q}_k + \bar{S}_k^{(2)}}{m\,(m+1)}. \tag{36}$$

$$\tilde{\eta}_k^{\text{i.i.d.}} = \frac{S_k^{(1)}}{m}, \quad \tilde{\eta}_k^{\text{s.c.},M_k \le L_k} = \frac{\bar{S}_k^{(1)}}{m}, \; \tilde{\eta}_k^{\text{s.c.},M_k > L_k} = \frac{\bar{S}_k^{(1)}}{m}. \tag{37}$$

$$\delta_{l,k}^{\text{i.i.d.}} = \frac{\beta_{k,l,k}}{\tilde{\eta}_k^{\text{i.i.d.}}} \varrho_{l,k}^{\text{i.i.d.}}, \quad \delta_{l,k}^{\text{s.c.},M_k \le L_k} = \frac{\beta_{k,l,k}}{\tilde{\eta}_k^{\text{s.c.},M_k \le L_k}} \varrho_{l,k}^{\text{s.c.},M_k \le L_k}, \; \delta_{l,k}^{\text{s.c.},M_k > L_k} = \frac{\beta_{k,l,k}}{\tilde{\eta}_k^{\text{s.c.},M_k > L_k}} \varrho_{l,k}^{\text{s.c.},M_k > L_k}. \tag{38}$$

in (39) must be evaluated separately, as demonstrated in the following theorem.

Theorem 3: In the presence of cell-wide coordination, the expected value of ICI (second term of (39)) for terminal l in cell k is given by

$$\mathbb{E}\left[|\mathbf{h}_{j,l,k}\boldsymbol{g}_{q,j}|^2\right] = \mathbb{E}\left[\boldsymbol{g}_{q,j}^{\text{H}}\boldsymbol{R}_j\boldsymbol{g}_{q,j}\right] = \frac{1}{L_j}\sum\nolimits_{i=1}^{M_j}\theta_i^2 f_i^2, \tag{42}$$

where θ_i is the i-th eigenvalue of $\boldsymbol{R}_j$ and f_i for $i = \{1, \ldots, M_j\}$ is derived in Appendix E.

Proof: One can regonize that $\mathbb{E}\left[|\boldsymbol{h}_{j,l,k}\boldsymbol{g}_{q,j}|^2\right] = \mathbb{E}\left[\boldsymbol{g}_{q,j}^{\text{H}}\boldsymbol{R}_j\boldsymbol{g}_{q,j}\right] = \text{tr}\left[\boldsymbol{R}_j\mathbb{E}\left[\boldsymbol{g}_{q,j}\boldsymbol{g}_{q,j}^{\text{H}}\right]\right]$. Now, $\mathbb{E}\left[\boldsymbol{g}_{q,j}\boldsymbol{g}_{q,j}^{\text{H}}\right] = \frac{1}{L_j}\mathbb{E}\left[\boldsymbol{G}_j\boldsymbol{G}_j^{\text{H}}\right]$, as the columns of $\boldsymbol{G}_j$ are identically distributed. Expressing $\boldsymbol{G}_j = \boldsymbol{H}_j^{\text{H}}\left(\boldsymbol{H}_j\boldsymbol{H}_j^{\text{H}} + \xi_j\boldsymbol{I}_{L_j}\right)^{-1}$ and identifying that $\boldsymbol{H}_j = \boldsymbol{U}_j\boldsymbol{R}_j^{\frac{1}{2}}$, we denote $\boldsymbol{V}_j = \boldsymbol{U}_j\boldsymbol{\Phi}_j$ and decompose $\boldsymbol{R}_j = \boldsymbol{\phi}_j\boldsymbol{\theta}_j\boldsymbol{\phi}_j^{\text{H}}$, where $\boldsymbol{\theta}_j = \text{diag}\left[\theta_1, \ldots, \theta_{M_j}\right]$ giving

$$\mathbb{E}\left[\boldsymbol{g}_{q,j}^{\text{H}}\boldsymbol{R}_j\boldsymbol{g}_{q,j}\right] = \frac{1}{L_j}\text{tr}\left[\boldsymbol{\phi}_j^{\text{H}}\boldsymbol{R}_j^2\boldsymbol{\phi}_j\mathbb{E}\left[\boldsymbol{V}_j\left(\boldsymbol{V}_j\boldsymbol{\theta}_j\boldsymbol{V}_j^{\text{H}} + \xi_j\boldsymbol{I}_{L_j}\right)^{-2}\boldsymbol{V}_j\right]\right]. \tag{43}$$

Noting that the expectation in (43) results in a diagonal matrix containing $f_1, \ldots, f_{M_j}$ yields the desired expression in (42), where f_i is derived in Appendix E. ■

C. Expected Per-User SINR and Ergodic Per-Cell Spectral Efficiency

The expected SINR in (25) can now be written as a function of $\delta_{l,k}$, $\iota_{l,k}$, $\tilde{\eta}_k$ and $\tilde{\eta}_j$. That is,

$$\begin{aligned}
\mathbb{E}\left[\rho_{l,k}^{\text{i.i.d.}}\right] &\approx \frac{\delta_{l,k}^{\text{i.i.d.}}}{\sigma_l^2 + \iota_{l,k}^{\text{i.i.d.}}} \\
\mathbb{E}\left[\rho_{l,k}^{\text{s.c.}M_k \le L_k}\right] &\approx \frac{\delta_{l,k}^{\text{s.c.}M_k \le L_k}}{\sigma_l^2 + \iota_{l,k}^{\text{s.c.}M_k \le L_k}} \\
\mathbb{E}\left[\rho_{l,k}^{\text{s.c.}M_k > L_k}\right] &\approx \frac{\delta_{l,k}^{\text{s.c.}M_k > L_k}}{\sigma_l^2 + \iota_{l,k}^{\text{s.c.}M_k > L_k}},
\end{aligned} \tag{44}$$

for the i.i.d. and semi-correlated cases, respectively. The expected SINRs can be translated into an approximation for the ergodic spectral efficiency of cell k by following (26), giving

$$\mathbb{E}\left[\text{R}_{\text{sum},k}^{\text{i.i.d.}}\right] \approx \sum\nolimits_{l=1}^{L_k}\log_2\left(1 + \mathbb{E}\left[\rho_{l,k}^{\text{i.i.d.}}\right]\right), \tag{45}$$

for the i.i.d. and equivalently for the semi-correlated scenarios. Having derived the expected SINR and ergodic sum spectral efficiency approximations, we evaluate their accuracy with the coordination strategies discussed in Section III-D, for a two-tier small-cell system in Section VI.

V. High SNR ZF Approximation With Unequal Spatial Correlation Matrices

In this section, we derive new results for the expected per-terminal SINR and ergodic per-cell spectral efficiency with unequal spatial correlation matrices for each terminal. For tractability of analysis, we consider the high SNR regime, where we can approximate the results for RZF with those for ZF precoding. We focus on the case of network-wide coordination, where the terminal correlation matrices follow the model in [24], which considers an exponential structure with a complex correlation co-efficient, φ, where $|\varphi|$ (magnitude of φ) captures the effects of inter-element spacing at the BS and a unique phase, assumed uniform on $[a, b]$, some subset of $[0, 2\pi]$ is used to differentiate the terminals. The channel from BS k to terminal l in cell j with a terminal specific correlation matrix is given by $\boldsymbol{h}_{k,l,j} = \boldsymbol{u}_{k,l,j}\boldsymbol{R}_{k,l,j}^{\frac{1}{2}}$, as defined in Section III-A.

With network-wide coordination, the $\sum_{i=1}^{K} L_i \times M_k$ composite channel matrix, $\boldsymbol{H}_k \triangleq \left[\boldsymbol{Z}_1^{\text{T}}, \boldsymbol{Z}_2^{\text{T}}, \ \ldots, \boldsymbol{Z}_K^{\text{T}}\right]^{\text{T}}$, where $\boldsymbol{Z}_k$ denotes the downlink channel to all terminals in cell k, given by $\boldsymbol{Z}_k \triangleq \left[\boldsymbol{h}_{k,1,k}^{\text{T}}, \ldots, \boldsymbol{h}_{k,L_k,k}^{\text{T}}\right]^{\text{T}}$. We note that $\boldsymbol{Z}_k$ has an identical form to (22). The corresponding $M_k \times L_k$ un-normalized ZF precoding matrix is defined as $\boldsymbol{G}_k \triangleq \left[\boldsymbol{H}_k^{\text{H}}\left(\boldsymbol{H}_k\boldsymbol{H}_k^{\text{H}}\right)^{-1}\right]_{X:Z}$ for the L_k terminals located in cell k with $X = \sum_{i=1}^{k-1} L_i + 1$ and $Z = \sum_{i=1}^{k} L_i$. The notation $[\boldsymbol{A}]_{X:Z}$ denotes columns X to Z of $\boldsymbol{A}$. We normalize the ZF matrix for cell k by $\eta_k \triangleq ||\boldsymbol{G}_k||_{\text{F}}^2/L_k$. As $\boldsymbol{H}_k\boldsymbol{G}_k = \left[\boldsymbol{H}_k\boldsymbol{H}_k^{\text{H}}\left(\boldsymbol{H}_k\boldsymbol{H}_k^{\text{H}}\right)^{-1}\right]_{X:Z} = [0, \ldots, \boldsymbol{I}_{X:Z}, \ldots, 0]^{\text{T}}$, perfect cancellation of IUI and ICI takes place allowing us to express the received signal at terminal l in cell k as

$$y_{l,k} = \sqrt{\frac{\beta_{k,l,k}}{\eta_k}}s_{l,k} + \bar{v}_l, \tag{46}$$

where $\beta_{k,l,k}$, $s_{l,k}$ and $\bar{v}_l$ are as defined in (19) and (18), respectively. With uniform power allocation and recognizing that $\mathbb{E}\left[|s_{l,k}|^2\right] = 1$, the received SNR for terminal l is given in [14]

$$\rho_{l,k}^{\text{ZF}} = \frac{\beta_{k,l,k}}{\sigma_l^2\eta_k} = \frac{\beta_{k,l,k}}{\sigma_l^2\text{tr}_{X:Z}\left[\left(\boldsymbol{H}_k\boldsymbol{H}_k^{\text{H}}\right)^{-1}\right]}, \tag{47}$$

where $\mathrm{tr}_{X:Z}[\boldsymbol{A}]$ represents the trace of the diagonal block of $\boldsymbol{A}$ involving rows and columns X to Z. To avoid computing the inverse in (47), we approximate $\left(\boldsymbol{H}_k\boldsymbol{H}_k^{\mathrm{H}}\right)^{-1}$ with a classical order N Neumann series (NS) as in [37] and denote $\boldsymbol{H}_k\boldsymbol{H}_k^{\mathrm{H}} = M_k\boldsymbol{I}_{\sum_{i=1}^{K}L_i} + \boldsymbol{\Delta}_k$. Hence, $\boldsymbol{\Delta}_k = \boldsymbol{H}_k\boldsymbol{H}_k^{\mathrm{H}} - M_k\boldsymbol{I}_{\sum_{i=1}^{K}L_i}$ with $\mathbb{E}[\boldsymbol{\Delta}_k] = 0$, allowing us to express

$$\left(\boldsymbol{H}_k\boldsymbol{H}_k^{\mathrm{H}}\right)^{-1} \approx \frac{1}{M_k}\sum_{p=0}^{N}(-1)^p\left(\frac{\boldsymbol{\Delta}_k}{M_k}\right)^p = \frac{1}{M_k}\sum_{p=0}^{N}\sum_{i=0}^{p}\binom{p}{i}\frac{(-1)^i}{(M_k)^i}\left(\boldsymbol{H}_k\boldsymbol{H}_k^{\mathrm{H}}\right)^i. \quad (48)$$

Substituting (48) into (47) yields

$$\rho_{l,k}^{\mathrm{ZF}} \approx \frac{\beta_{k,l,k}}{\sigma_l^2\mathrm{tr}_{X:Z}\left[\frac{1}{M_k}\sum_{p=0}^{N}\sum_{i=0}^{p}\binom{p}{i}\frac{(-1)^i}{(M_k)^i}\left(\boldsymbol{H}_k\boldsymbol{H}_k^{\mathrm{H}}\right)^i\right]}. \quad (49)$$

From (49), the expected SNR of terminal l in cell k can be approximated as

$$\mathbb{E}\left[\rho_{l,k}^{\mathrm{ZF}}\right] \approx \frac{\beta_{k,l,k}}{\sigma_l^2\frac{1}{M_k}\sum_{p=0}^{n}\sum_{i=0}^{p}\binom{p}{i}\frac{(-1)^i}{M_k^i}\mathbb{E}\left[\mathrm{tr}_{X:Z}\left[\left(\boldsymbol{H}_k\boldsymbol{H}_k^{\mathrm{H}}\right)^i\right]\right]}, \quad (50)$$

using the univariate special case of the first-order Delta expansion motivated in Remark 2. In what follows, with a two-term NS (i.e., $N = 2$), we present a closed-form expression of (50).

Theorem 4: When $\boldsymbol{h}_{k,l,j} = \boldsymbol{u}_{k,l,j}\boldsymbol{R}_{k,l,j}^{\frac{1}{2}}$, where $\boldsymbol{u}_{k,l,j} \sim \mathcal{CN}\left(0, \boldsymbol{I}_{M_k}\right)$ and $\boldsymbol{R}_{k,l,j}$ is a terminal specific transmit spatial correlation matrix, the RZF expected per-terminal SINR can be approximated with a ZF expected per-terminal SNR with the use of a two-term NS in the high SNR regime. For the l-th terminal in cell k being served by BS k, this is given by

$$\mathbb{E}\left[\rho_{l,k}^{\mathrm{ZF}}\right] \approx \frac{\beta_{k,l,k}\,(M_k)^3}{\sigma_l^2\left[L_k\,(M_k)^2 + \left[L_k\sum_{k=1}^{K}L_k\mathrm{tr}_{X:Z}\left[\bar{\boldsymbol{R}}\bar{\boldsymbol{R}}_k\right]\right]\right]}, \quad (51)$$

where $\bar{\boldsymbol{R}} \triangleq \frac{\sum_{j=1}^{K}\sum_{l=1}^{L_j}\boldsymbol{R}_{k,l,j}}{\sum_{j=1}^{K}L_j}$ is the average correlation matrix of all terminals in the system and $\bar{\boldsymbol{R}}_k \triangleq \frac{\sum_{l=1}^{L_k}\boldsymbol{R}_{k,l,k}}{L_k}$ is the average correlation matrix for the terminals in cell k, respectively.

Proof: See Appendix F. ∎

Following (45), the expected per-terminal SNR can be easily translated to the ergodic per-cell sum spectral efficiency. We verify the accuracy of Theorem 4 in Section VI, where we also present comparisons of the expected SINR and ergodic sum spectral efficiency with those obtained by having an equal correlation matrix at all terminals.

Remark 6: Theorem 4 provides a closed-form approximation to an extremely complex situation where all terminals have unequal correlation matrices. The structure of (51) demonstrates the impact of unequal correlation matrices, primarily through $\mathrm{tr}_{X:Z}\left[\bar{\boldsymbol{R}}\bar{\boldsymbol{R}}_k\right]$. It is straight forward to show that this partial trace tends to maximize as $\bar{\boldsymbol{R}}_k$ approaches $\bar{\boldsymbol{R}}$, the case of equal correlation matrices, maximizing the expected noise power, thereby reducing the expected ZF SNR. As a result of this, the SNR performance of equal correlation matrices tend to act as a lower bound on the performance of such systems. Moreover, fixing the partial trace in the denominator of (51), along with the other propagation parameters, the effects of increasing M_k and L_k can be readily observed from the expression. Firstly, increasing M_k with L_k fixed increases the expected signal power cubically, while increasing the expected noise power quadratically, resulting in a net increase in the expected signal power of $\mathcal{O}(M_k)$. On the other hand, fixing M_k and increasing L_k leads to an exponential amplification of the expected noise power by $\mathcal{O}\left(1/L_k + KL_k^2\right)$, while the signal power remains unaltered. For both cases, $\mathcal{O}(\cdot)$ denotes the "order" notation.

VI. Numerical Results

We consider a two-tier network of macro and microcells. Unless otherwise specified, the simulation parameters were been obtained from [38]. Net transmit powers of macrocell k and microcell j, $P_{\mathrm{t},k}$ and $P_{\mathrm{t},j}$ are 46 dBm and 30 dBm, respectively. Large-scale propagation effects of geometric attenuation and shadow-fading follow the model in (19), where for $d_0 = 1$ m, $\varsigma = 31.54$ dB [29]. The decay exponents $\alpha_k = 4$ and $\alpha_j = 3.5$, whilst the shadow-fading standard deviation, $\sigma_{\mathrm{s}} = 8.0$ dB. Without loss of generality, the noise power at terminal l in cell k is unity, i.e., $\sigma_l^2 = 1$. Circular cell radii of 1 km and 70 m are assumed for cell k and j, respectively. The location of BS k remains fixed, whilst the location of BS j varies depending on the scenario considered (discussed later). We constrain the placement of BS j outside a 70 m exclusion radius from BS k. The total number of single-antenna terminals being served by BSs k and j are $L_k = 5$ and $L_j = 3$, which are distributed uniformly over the area of the respective cells. The number of serving antennas at BSs k and j (M_k and M_j) vary depending on the scenario considered ($M_k, M_j > L_k, L_j$ or $M_k, M_j \leq L_k, L_j$). For the former, $M_k = 8$, $M_j = 4$ and for the latter, $M_k = 4$, $M_j = 2$, respectively.[2] With equal correlation matrices, we model the presence of spatial correlation at BSs k and j with the Kronecker model, where $(\boldsymbol{R}_k)_{x,z} = \left(\boldsymbol{R}_j\right)_{x,z} = \varphi^{|x-z|}$ for $x, z \in \{1, \ldots, M_k\}$ and $\in \left\{1, \ldots, M_j\right\}$ has an exponential structure [26]. On the other hand, when each terminal is assigned an unequal correlation matrix, we employ the model in [24] where each correlation matrix has a structure proportional to $\varphi^{|x-z|}$ modeling the inter-element spacing and an independent $[0, 2\pi]$ uniformly distributed phase component is multiplied modeling the terminal distribution in a cell. We assess the performance of the system with equal and unequal correlation matrices in Sections VI-B and VI-C, respectively.

A. Simulation Settings

An arbitrary network of 11 BSs comprising of 1 macro and 10 microcells is considered, unless otherwise specified. Uniform, cell-edge and cell-centric microcell placements within the macrocell is considered, as shown in Figs. 2(a), 2(b) and 2(c), respectively. For cell-edge and cell-centric placements, we restrict the microcells outside the

[2]With $M_k \leq L_k$, BS k tries to serve more terminals than the number of transmit antennas. In practice, such systems rely on user scheduling mechanisms to decide on the suitable operating conditions.

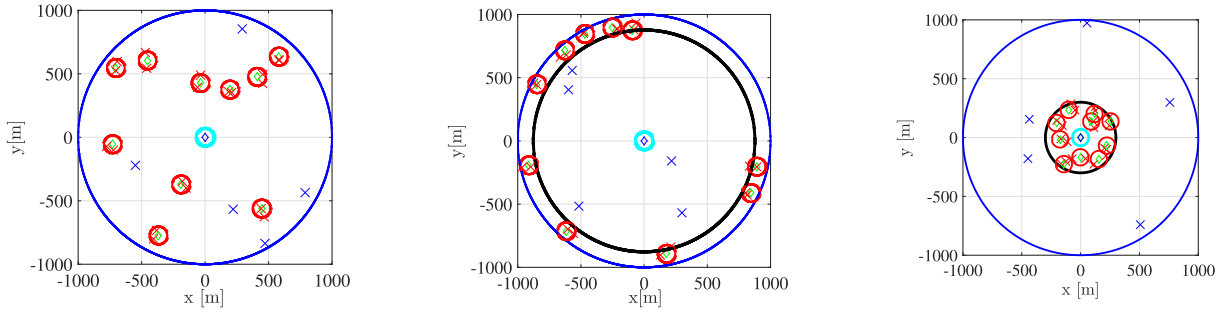

(a) Uniform microcells (b) Cell-edge microcells (c) Cell-centric microcells

Fig. 2. Varying microcell placements. (a) Uniform microcells. (b) Cell-edge microcells. (c) Cell-centric microcells.

cell-edge and inside the cell-centric exclusion areas, marked with black circles in Figs. 2(b) and 2(c). These exclusion zones were numerically determined using the 10-th and 90-th percentiles of the cumulative distribution function (CDF) of the received SNR (defined later) for a macro terminal. In particular, the cell-edge of a macrocell was identified as 877 m to 1000 m from the center and the cell-center was identified from the origin of the macrocell to 230 m.[3] The 70 m macro exclusion zones are marked with cyan circles in Figs. 2(a), 2(b) and 2(c). The microcells are denoted with red circles with its associated terminals denoted with red crosses. Likewise, terminals associated to the macro BS are marked with blue crosses. Finally, macro and micro BSs are denoted with blue and green diamonds.

The results in subsection B include evaluation of the simulated and approximated expected SINR and ergodic sum spectral efficiency in (25), (44), (26) and (45) for i.i.d. and semi-correlated channels, respectively with equal correlation matrices. In subsection C, with unequal correlation matrices, we evaluate the expected SNR performance of (51) and translate this to approximate the ergodic spectral efficiency as shown in (45). We obtain all results using 10^5 independent trials with the coordination strategies discussed in Section III-D. We define SNR as the ratio of the average received signal power to the receiver noise power.[4]

B. Tightness of Expected SINR and Ergodic Spectral Efficiency

Fig. 3 shows the expected SINR ($\mathbb{E}[\rho]$) CDF of a macro terminal with cell-centric, cell-edge and uniform microcell placements at SNR=10 dB with $\varphi = 0$ and $M \leq L$. The expectation is performed over the fast-fading with the distribution representing the randomness in terminal position and shadow-fading. We consider the case with no microcells as a baseline. The cell-centric microcell placement results in the best macro user SINR performance, as the terminals are distributed uniformly over the macrocell coverage area and thus have higher probability of being further away from the micro

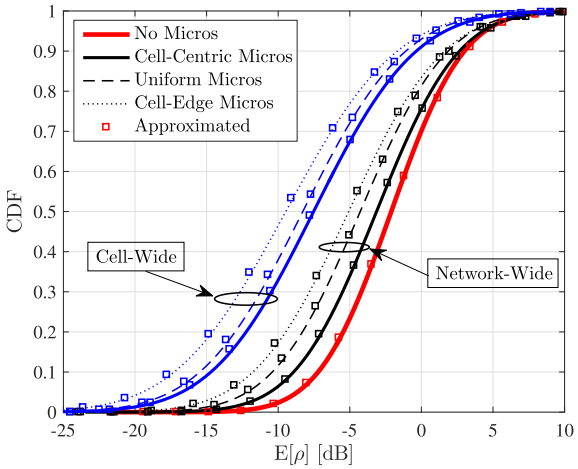

Fig. 3. CDF of $\mathbb{E}[\rho]$ for a macrocell terminal at SNR=10 dB with $\varphi = 0$ and $M \leq L$.

BSs, resulting in less ICI. This is followed by uniform and cell-edge placements, which often result in closer proximity to a typical macro terminal, having an adverse effect on its SINR. The SINR gains of network-wide coordination relative to cell-wide coordination are more prominent in the lower half of the CDF (<0.5), where the combined effects of noise with IUI and ICI dominate.[5] In contrast, at higher probabilities (>0.9), the spread between the extreme cases of cell-centric microcells with network-wide coordination and cell-edge microcells with cell-wide coordination becomes narrower, due to the reduction in IUI and ICI relative to the signal power. This in-turn suggests that the cell-edge rates of the system (<0.1) may have higher variability than the peak-rates of the system (>0.9) and will benefit more from coordination. We also observe that in all cases, the derived SINR approximations closely follow the simulated responses over the entire probability range.

Fig. 4 shows an equivalent CDF of a typical micro terminal. Here, we consider the case of a single microcell in the macro coverage area as the baseline. Naturally, all three coordination strategies are applicable to the micro terminal. As expected,

[3]The cell-edge and cell-centric exclusion zones are sensitive to the chosen numerical parameters.

[4]The averaging in the received signal power is performed over the large-scale fading parameters.

[5]For the typical macro terminal, cell-wide and macro-only coordination result in equal performance due to the nature of the respective coordination strategies. Thus, for clarity, the expected SINR distributions with macro-only coordination are omitted.

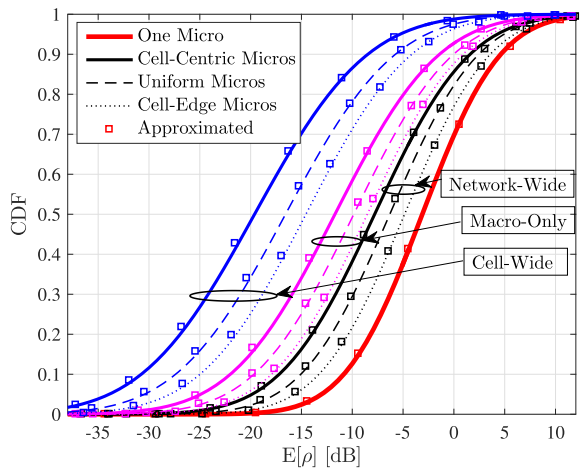

Fig. 4. CDF of $\mathbb{E}[\rho]$ for a microcell terminal at SNR=10 dB with $\varphi = 0$ and $M \leq L$.

the opposite trend to that in Fig. 3 is seen, where the cell-edge microcell placement results in superior performance, followed by uniform and cell-centric placements, where ICI from the macrocell is likely to be higher. At probability 0.5, irrespective of the microcell placement, macro-only and cell-wide coordination strategies reduce the expected SINR by approximately 4 dB and 10 dB relative to network-wide coordination, as the CDFs exhibit parallel behavior. As before, higher variability in the SINRs can be seen at lower probabilities and the derived SINR approximations are seen to remain tight against the simulated equivalents.

Keeping all other propagation parameters the same, we now consider the case of $M > L$, where we first evaluate the expected SINR and ergodic sum spectral efficiency approximation accuracy. For the sake of clarity, we consider a typical macrocell terminal and focus on the specific case of network-wide BS coordination with cell-centric and cell-edge microcell placements.[6] With increasing numbers of serving antennas at the macro BS and a fixed number of terminals in both macro and microcells, Fig. 5 demonstrates the expected SINR and ergodic sum spectral efficiency performance. An increase in the expected SINR and ergodic sum spectral efficiency is observed for both microcell placements, at the cost of increasing the spatial d.o.f. (as a result of more serving antennas), which allows for better ICI control via coordinated RZF. Both the approximations are seen to become tighter with increasing numbers of service antennas. This is due to the quadratic forms in the numerator and denominator of (25) (and therefore (26)) averaging their individual components, providing the variance reduction required relative to their mean. To precisely characterize the accuracy of both approximations, a relative absolute approximation error as a percentage can be defined, such that $\text{Error}_{\mathbb{E}[\rho_{l,k}]}[\%] = |(\text{True} - \text{Approx.})/(\text{True})| \times 100$. Moreover, Fig. 5 also depicts the approximation accuracy as a percentage. While increasing the macro service antennas exponentially vanishes the approximation error, a very small error is observed at lower numbers of service antennas. For the expected SINR, an approximation accuracy of 5% is achieved with $M = 8$, while for the ergodic sum spectral efficiency, a 5% error corresponds to $M = 4$ (both indicated on Fig. 5's lowest two subplots with green diamonds). The reduction in the spectral efficiency approximation error is due to the logarithm in the spectral efficiency calculation, providing further averaging on the expected SINR approximation.

With $M > L$, the improvement in the expected per-terminal SINR as a function of SNR is demonstrated in Fig. 6 for a typical macro terminal. Here, the averaging is performed globally over the link gains, as well as the multi-path fading, denoted by $\mathbb{E}_{\beta,\boldsymbol{h}}[\cdot]$.

The analytical expressions remain tight throughout the entire SNR range considered. The baseline case of no microcells demonstrates a near linear increase in the expected SINR with increasing SNR, as the serving antennas at the macro BS exceeds the total number of terminals, nulling the IUI. The remaining cases with cell-wide and network-wide coordination still suffer from ICI, saturating the SINR in the high SNR regime. Under semi-correlated Rayleigh fading, the expected per-terminal SINR is seen to degrade with increasing levels of spatial correlation at the BS. Fig. 7 shows the expected SINR of a macro terminal as a function of spatial correlation, φ. While varying φ from $0 - 0.6$ has very little effect on the expected SINR, from $\varphi = 0.7$ onwards, a heavy penalty in the expected SINR is paid due to a greater reduction in the usable spatial d.o.f. This trend is visible for all microcell placements irrespective of the coordination strategy. The reduction in the spatial d.o.f. can alternatively be interpreted as an increase in the IUI, thus decreasing the per-terminal SINR. Although not shown, the same trend in the degradation of expected per-user SINR can be observed for a micro terminal. For all cases, our analytical approximations remain tight even for extremely high levels of channel correlation.

Figs. 8 and 9 demonstrate the ergodic per-cell sum spectral efficiency distributions ($\mathbb{E}[\text{R}_{\text{sum}}]$) for the macro and a given microcell, following (26) and (45), respectively. For the macrocell, higher variability in the peak rates is observed in comparison to cell-edge and median rates, as the combined effect of IUI and ICI impacts performance. Equivalently, for the typical microcell, higher variability in the cell-edge, median and peak rates demonstrates its sensitivity to the aggregate interference and its location within the macrocell. This suggests that the cell-edge, median and peak-rates will benefit from BS coordination.

C. Impact of Unequal Correlation Matrices

We now consider a network of 4 BSs composing of 1 macro and 3 overlaid microcells. Keeping the same constraints in the microcell placements as in subsection B, we evaluate the performance of the system with network-wide coordination where each terminal is assigned an unequal correlation matrix capturing the effects of inter-element spacing at the BS and terminal locations in the cell. Following the model described in Section V, for each subsequent result, we consider $|\varphi| = 0.9$ with uniformly distributed phase on $[0, 2\pi]$. As ZF precoding

[6]Since the trends resulting from the three types of microcell placements are identical for further results considered, to enhance legibility, the subsequent figures only include cell-edge and cell-centric placements, respectively.

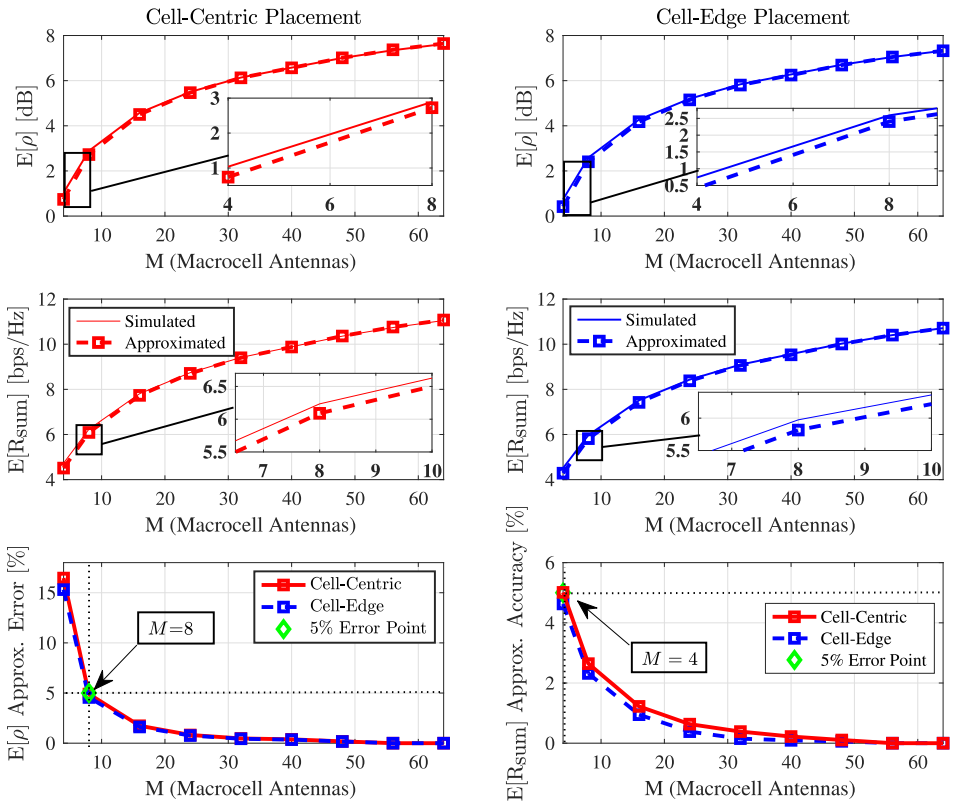

Fig. 5. $\mathbb{E}[\rho]$, $\mathbb{E}[\mathrm{R_{sum}}]$ and approximation accuracy for a typical macrocell terminal vs. the number of macro BS antennas. Note that $M > L$ and SNR=10 dB with $\varphi = 0$.

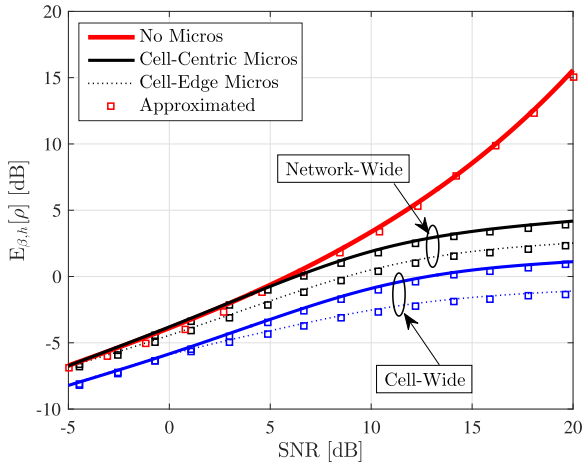

Fig. 6. $\mathbb{E}_{\beta,\boldsymbol{h}}[\rho]$ vs. SNR of a macro terminal with $M > L$ and $\varphi = 0$.

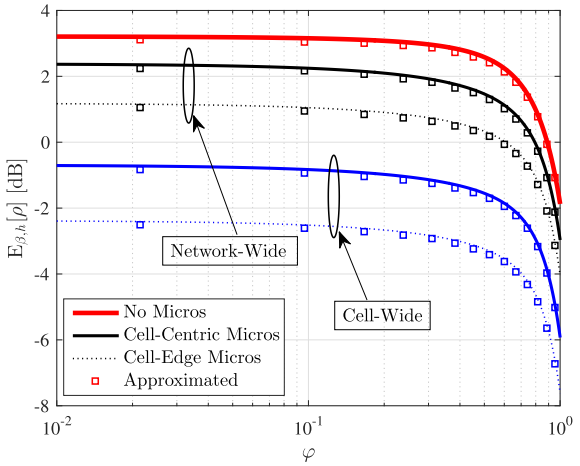

Fig. 7. $\mathbb{E}_{\beta,\boldsymbol{h}}[\rho]$ vs. φ for a macro terminal at SNR=10 dB with $M > L$.

is employed, we consider 16 and 10 antennas at macro and micro BSs serving 3 macro and 2 microcell terminals.

Figs. 10 and 11 show the expected per-terminal SNR for the typical macro and microcell terminals. Due to zero interference, and the relatively large number of serving antennas in comparison to the number of terminals, a significant increase in the macro and micro terminal SINRs can be observed. In such scenarios, where interference is not the performance limiting factor, the need for coordination is less convincing than in previous cases. For both the macro and micro terminals, varying the microcell placements has a very minor impact on their SINRs. The two-term NS approximations to the expected ZF per-terminal SNR is seen to remain tight for all coordination mechanisms in both Figs. 10 and 11, respectively. A comparison to the RZF expected per-terminal SINR is made in the baseline cases of no micros and one micro in Figs. 10 and 11, where ZF expected SNR is shown to closely match the RZF performance. Also, the expected SNR performance with unequal correlation matrices is superior in Figs. 10 and 11 than the case where each terminal has

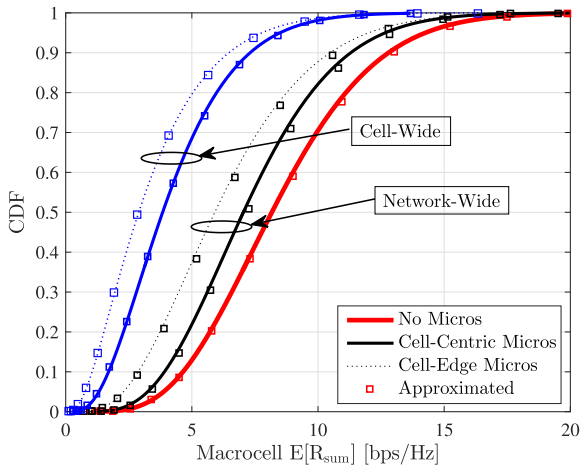

Fig. 8. Macrocell $\mathbb{E}[\mathrm{R_{sum}}]$ at SNR=10 dB with $M > L$ and $\varphi = 0$.

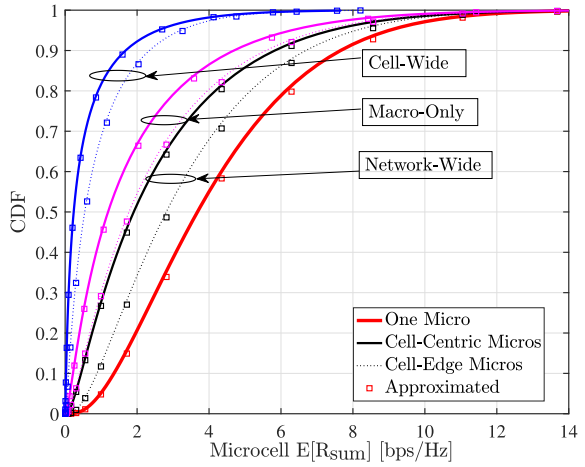

Fig. 9. Microcell $\mathbb{E}[\mathrm{R_{sum}}]$ at SNR=10 dB with $M > L$ and $\varphi = 0$.

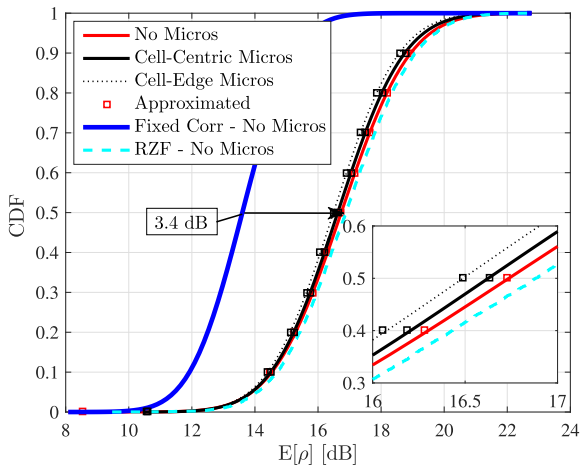

Fig. 10. CDF of $\mathbb{E}[\rho]$ for a macro terminal with unequal correlation matrices at SNR=10 dB.

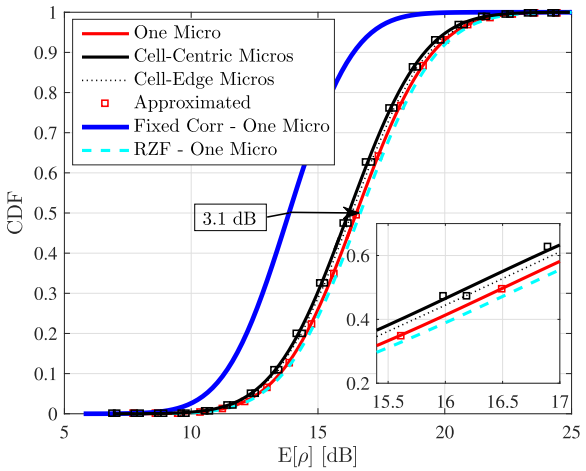

Fig. 11. CDF of $\mathbb{E}[\rho]$ for a micro terminal with unequal correlation matrices at SNR=10 dB.

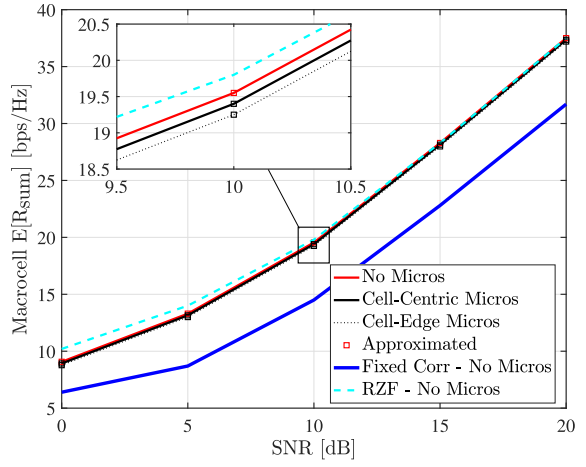

Fig. 12. Macrocell $\mathbb{E}[\mathrm{R_{sum}}]$ vs. SNR with unequal correlation matrices.

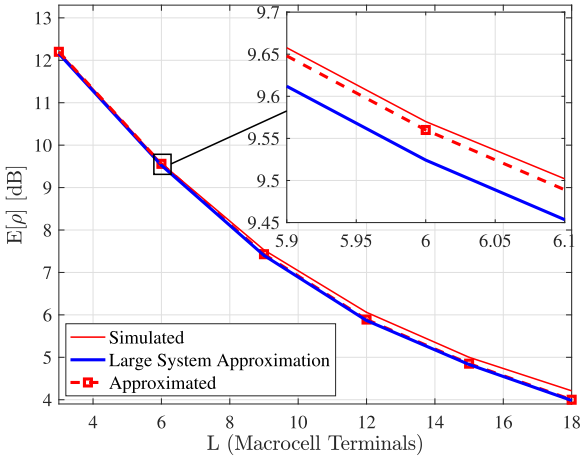

Fig. 13. Large system approx. comparison of $\mathbb{E}[\rho]$ vs. L with $M = 32$ and $L = 3, \ldots, 18$.

an equal correlation matrix, due to the denominator of (51) increasing, as predicted earlier in Remark 5. This gap is seen to translate into the ergodic spectral efficiency for the macrocell and remains approximately constant across the SNR range considered. This is shown in Fig. 12, where the derived approximations retain their tightness and are thus insensitive to changes in SNRs.

Finally, it is interesting to note that the remarkably simple, novel expression provided in (51) has a similar accuracy to that provided by limiting fixed point algorithms. For example, [22] provides an asymptotic single-cell solution which is implemented in Fig. 13 for the case of $M = 32$ antennas, serving $L \in \{3, \ldots, 18\}$ terminals in a macrocell where the correlation matrices are computed from [24] with $|\varphi| = 0.9$

and a uniformly distributed phase between $[0, 2\pi]$. As can be seen, our approach offers a small accuracy improvement and is an alternative approach if a single expression is preferred to a fixed point solution.

VII. Conclusion

A general analytical framework for characterizing the expected SINR and ergodic sum spectral efficiency of a multi-cellular system was presented. An application to two-tier small-cell networks was considered with varying degrees of coordinated RZF processing. Assuming both i.i.d. and semi-correlated Rayleigh fading, with equal correlation matrices, the analytical expressions were averaged over eigenvalue densities of the respective complex Wishart matrices. In the high SNR regime, with ZF precoding, closed-form expressions were derived to approximate the RZF expected SINR and ergodic spectral efficiency with unequal correlation matrices. Numerical results demonstrated the tightness of analytical expressions over a wide range of SNRs, spatial correlation levels and system dimensions. It was observed that the gains in the expected per-terminal SINR and ergodic spectral efficiencies were influenced by microcell locations and varying degrees of BS coordination, as they directly impacted the systems' ability to suppress ICI. Under semi-correlated fading, the expected SINR decreased with increasing levels of spatial correlation due to a loss in the usable spatial degrees of freedom. Expected SINR and ergodic spectral efficiencies with unequal correlation matrices were observed to be greater than the case with equal correlation matrices as demonstrated analytically.

Appendix A
Proof of Theorem 1

We begin with the fact that

$$S_k^{\mu} = \mathbb{E}_{\lambda}\left[\sum_{i=1}^{m} \frac{\lambda_i^{\mu}}{(\lambda_i + \xi_k)^2}\right] = m\left\{\int_0^{\infty} \frac{\lambda^{\mu}}{(\lambda + \xi_k)^2} f_0(\lambda)\, d\lambda\right\}, \tag{52}$$

where $\mathbb{E}_{\lambda}[\cdot]$ denotes the expectation over the eigenvalues and $f_0(\lambda)$ is the density of an arbitrary eigenvalue, λ, from $\{\lambda_1, \ldots, \lambda_m\}$. To evaluate (52) for an uncorrelated central Wishart matrix, we substitute (2) into (52), resulting in

$$S_k^{\mu} = m\left\{\frac{\lambda^{\mu}}{(\lambda + \xi_k)^2} \frac{1}{m} \sum_{i=1}^{m} \frac{(i-1)!}{(i-1+n-m)!} \lambda^{n-m} e^{-\lambda} \times \left(\sum_{z=0}^{i-1} (-1)^z \binom{i-1+n-m}{i-1-z} \frac{\lambda^z}{z!}\right)^2 d\lambda\right\}. \tag{53}$$

After some algebraic manipulation, we can write (53) as

$$S_k^{\mu} = \sum_{i=1}^{m} \frac{(i-1)!}{(i-1+n-m)!} \sum_{z=0}^{i-1} \sum_{\substack{l=0 \\ l \neq z}}^{i-1} (-1)^{z+l} \binom{i-1+n-m}{i-1-z}^2 \times \frac{1}{z!l!}\left\{\int_0^{\infty} \frac{\lambda^{\mu+n-m+z-l} e^{-\lambda}}{(\lambda + \xi_k)^2} d\lambda\right\}. \tag{54}$$

The integral in (54) has the form of $J_{a,b,c}(\xi_k)$ defined in (15), where $a = \mu + n - m + z - l$, $b = 2$ and $c = 1$. Following the solution provided in (17) yields the desired expression in (31).

Appendix B
Proof of Theorem 2

Substituting the arbitrary density defined in (7) into (52) results in

$$\bar{S}_k^{\bar{\mu}} = m\left\{\int_0^{\infty} \frac{\lambda_{\mathrm{sc}}^{\bar{\mu}}}{(\lambda_{\mathrm{sc}} + \xi_k)^2} \frac{1}{m \prod_{i<j}^{n} (\theta_j - \theta_i)} \sum_{l=1}^{n} \times \sum_{k=n-m+1}^{n} \frac{\lambda_{\mathrm{sc}}^{m+k-n-1} e^{-\lambda_{\mathrm{sc}}/\theta_l} \theta_l^{n-m-1}}{\Gamma(m-n+k)} \mathcal{D}_{l,k}\right\}. \tag{55}$$

Upon some simplification, we arrive at

$$\bar{S}_k^{\bar{\mu}} = \frac{1}{\prod_{i<j}^{n} (\theta_j - \theta_i)} \sum_{l=1}^{n} \sum_{k=n-m+1}^{n} \frac{\theta_l^{n-m-1} \mathcal{D}_{l,k}}{\Gamma(m-n+k)} \times \left\{\int_0^{\infty} \frac{\lambda_{\mathrm{sc}}^{m+k-n-1+\bar{\mu}} e^{-\lambda_{\mathrm{sc}}/\theta_l}}{(\lambda_{\mathrm{sc}} + \xi_k)^2} d\lambda_{\mathrm{sc}}\right\}, \tag{56}$$

where $\mathcal{D}_{l,k}$ and $\Gamma(m-n+k)$ are as defined in (7). The integral in (56) is of the form of $J_{a,b,c}(\xi)$ in (15), where $a = m + k - n - 1 + \bar{\mu}$, $b = 2$ and $c = \theta_l$, where θ_l is the l-th eigenvalue of $\boldsymbol{R}_k$. Substituting the result of (17) into the required integral yields the desired expression in (32).

Appendix C
Proof of Lemma 1

$$\begin{aligned} Q_k &= \mathbb{E}_{\lambda}\left[\left(\sum_{l=1}^{m} \frac{\lambda_l}{\lambda_l + \xi_k}\right)^2\right] = \mathbb{E}_{\lambda}\left[\sum_{l=1}^{m} \left(\frac{\lambda_l}{\lambda_l + \xi_k}\right)^2\right] \\ &\quad + \mathbb{E}_{\lambda}\left[\sum_{a=1}^{m} \sum_{\substack{b=1 \\ b \neq a}}^{m} \left(\frac{\lambda_a}{\lambda_a + \xi_k}\right)\left(\frac{\lambda_b}{\lambda_b + \xi_k}\right)\right], \\ &= m\mathbb{E}_{\lambda}\left[\frac{1}{m} \sum_{l=1}^{m} \left(\frac{\lambda_l}{\lambda_l + \xi_k}\right)^2\right] + m(m-1) \\ &\quad \times \left\{\mathbb{E}_{\lambda}\left[\frac{1}{m(m-1)} \sum_{a=1}^{m} \sum_{\substack{b=1 \\ b \neq 1}}^{m} \left(\frac{\lambda_a}{\lambda_a + \xi_k}\right)\left(\frac{\lambda_b}{\lambda_b + \xi_k}\right)\right]\right\}, \end{aligned} \tag{57}$$

where $\mathbb{E}_{\lambda}[\cdot]$ denotes expectation over the eigenvalues and λ_a, λ_b denote an arbitrary pair of eigenvalues. Via the result derived in Theorem 1, we can evaluate the first term in (57). By denoting the joint density of (λ_a, λ_b) as $f_0(\lambda_a, \lambda_b)$, we can write (57) as (58), shown on top of the next page. Using

$$Q_k = S_k^2 + m\,(m-1)\left\{\int_0^\infty\int_0^\infty \frac{\lambda_a}{\lambda_a+\xi_k}\frac{\lambda_b}{\lambda_b+\xi_k} f_0\,(\lambda_a,\lambda_b)\,d\lambda_b d\lambda_a\right\}. \tag{58}$$

$f_0\,(\lambda_a,\lambda_b)$ in (4) allows us to write (58) as

$$\begin{aligned} Q_k = {} & S_k^2 + m\,(m-1) \\ & \times \left\{\int_0^\infty\int_0^\infty \left(\frac{\lambda_a}{\lambda_a+\xi_k}\right)\left(\frac{\lambda_b}{\lambda_b+\xi_k}\right)\frac{1}{m\,(m-1)} \right. \\ & \times \sum_{i=1}^{m}\sum_{\substack{j=1\\ j\neq i}}^{m} (\lambda_a\lambda_b)^{n-m}\, e^{-(\lambda_a+\lambda_b)}\Phi \\ & \times \left(\kappa_{i-1}^{(n-m)}(\lambda_a)^2\,\kappa_{j-1}^{(n-m)}(\lambda_b)^2 - \kappa_{i-1}^{(n-m)}(\lambda_a)\,\kappa_{j-1}^{(n-m)}\right. \\ & \left.\left. \times\ (\lambda_a)\,\kappa_{i-1}^{(n-m)}\,(\lambda_b)\,\kappa_{j-1}^{(n-m)}\,(\lambda_b)\right) d\lambda_b d\lambda_a \right\}. \end{aligned} \tag{59}$$

After some simplifications, we can express (59) as

$$\begin{aligned} Q_k = {} & S_k^2 + \sum_{i=1}^{m}\sum_{\substack{j=1\\ j\neq i}}^{m}\Phi \\ & \times \left\{\int_0^\infty\int_0^\infty \frac{(\lambda_a\lambda_b)^{n-m+1}\, e^{-(\lambda_a+\lambda_b)}}{(\lambda_a+\xi_k)\,(\lambda_b+\xi_k)} \left(\kappa_{i-1}^{(n-m)}\,(\lambda_a)^2\right.\right. \\ & \times \kappa_{j-1}^{(n-m)}\,(\lambda_b)^2 - \kappa_{i-1}^{(n-m)}\,(\lambda_a)\,\kappa_{j-1}^{(n-m)}\,(\lambda_a) \\ & \left.\left. \times\ \kappa_{i-1}^{(n-m)}\,(\lambda_b)\right) d\lambda_b d\lambda_a \right\}, \end{aligned} \tag{60}$$

where Φ is as defined in (5). The integrals in (60) can be split into two parts, as shown in (61) on top of the next page. As the double integrals in (61) are of the same function with different variables, we can write (61) by squaring the result of a single integral, such that

$$\begin{aligned} Q_k = {} & S_k^2 + \sum_{i=1}^{m}\sum_{\substack{j=1\\ j\neq i}}^{m}\Phi \\ & \times \left\{\left(\sum_{f=0}^{i-1}\sum_{\substack{z=0\\ z\neq f}}^{i-1}(-1)^{f+z}\binom{n-m+i-1}{i-1-f}\right.\right. \\ & \times \binom{n-m+i-1}{i-1-z}\frac{1}{f!z!}\int_0^\infty \frac{e^{-\lambda}\lambda^{n-m+1+f+z}}{\lambda+\xi_k}d\lambda\Bigg)^2 \\ & - \left(\sum_{f=0}^{i-1}\sum_{\substack{z=0\\ z\neq f}}^{i-1}(-1)^{f+z}\binom{n-m+i-1}{i-1-f}\right. \\ & \times \binom{n-m+j-1}{j-1-z} \\ & \left.\left. \times\ \frac{1}{f!z!}\int_0^\infty \frac{e^{-\lambda}\lambda^{n-m+1+f+z}}{\lambda+\xi_k}d\lambda\right)^2\right\}. \end{aligned} \tag{62}$$

Recognizing that the integrals in (62) have the same form as $J_{n-m+1+f+z,1,1}\,(\xi_k)$ and substituting the solution of (15) in (62) yields the desired expression in (33).

Appendix D
Proof of Lemma 2

We begin by substituting the result in Corollary 1 into (58) where Q_k and S_k are replaced by their correlated central counterparts in $\bar{Q}_k$ and $\bar{S}_k$ giving

$$\begin{aligned} \bar{Q}_k = {} & \bar{S}_k^2 + m\,(m-1) \\ & \times \left\{\int_0^\infty\int_0^\infty \left(\frac{\lambda_a}{\lambda_a+\xi_k}\right)\left(\frac{\lambda_b}{\lambda_b+\xi_k}\right)\hat{\chi}\right. \\ & \times \sum_{i=0}^{m-1}\sum_{\substack{j=0\\ j\neq i}}^{m-1}(-1)^{i+j-p(i,j)}\,\lambda_1^{i+n-m}\,\lambda_2^{j+n-m} \\ & \times \sum_{k=1}^{m}\sum_{\substack{l=1\\ l\neq k}}^{m}(-1)^{k-1}\times e^{-\lambda_a/\theta_k}\,(-1)^{l-p(l)} \\ & \left.\times\ e^{-\lambda_2/\theta_l}\det\,(\Xi)_{i,j;k,l}\,d\lambda_b d\lambda_a\right\}, \end{aligned} \tag{63}$$

where $\hat{\chi}$, $p\,(i,j)$, $p\,(l)$ and Ξ are as defined in (8) and (10). After some mathematical simplifications, we are able to write (63) as

$$\begin{aligned} \bar{Q}_k = {} & \bar{S}_k^2 + \hat{\chi}\sum_{i=0}^{m-1}\sum_{\substack{j=0\\ j\neq i}}^{m-1}\sum_{k=1}^{m}\sum_{\substack{l=1\\ l\neq k}}^{m}(-1)^{i+j-p(i,j)} \\ & \times (-1)^{k-1+l-p(l)}\det\,(\Xi)_{i,j;k,l} \\ & \times \left\{\int_0^\infty \frac{e^{-\lambda_a/\theta_k}\lambda_a^{i+n-m+1}}{\lambda_a+\xi_k}d\lambda_a \int_0^\infty \frac{e^{-\lambda_b/\theta_l}\lambda_b^{j+n-m+1}}{\lambda_b+\xi_k}d\lambda_b\right\}. \end{aligned} \tag{64}$$

The integrals in (64) are of the same form, with varying powers of i and j for λ_a and λ_b. Their general solution is presented in (15). Upon substituting the solution of the integrals in (64) yields the expression in Lemma 2.

Appendix E
Calculation of f_i in (42)

Denoting $\boldsymbol{V}_j = \left[\boldsymbol{v}_1,\ldots,\boldsymbol{v}_{M_j}\right]$, we recognize that

$$\begin{aligned} f_i &= \mathbb{E}\left[\boldsymbol{v}_i\left(\boldsymbol{V}_j\boldsymbol{\theta}_j\boldsymbol{V}_j^{\mathrm{H}} + \xi_j\boldsymbol{I}_{L_j}\right)^{-2}\boldsymbol{v}_i\right] \\ &= -\frac{\partial}{\partial\xi_j}\mathbb{E}\left[\boldsymbol{v}_i^{\mathrm{H}}\left(\boldsymbol{V}_j\boldsymbol{\theta}_j\boldsymbol{V}_j^{\mathrm{H}} + \xi_j\boldsymbol{I}_{L_j}\right)^{-1}\boldsymbol{v}_i\right], \end{aligned} \tag{65}$$

$$Q_k = S_k^2 + \sum_{i=1}^{m}\sum_{\substack{j=1\\ j\neq i}}^{m} \Phi\left\{ \int_0^{\infty}\int_0^{\infty} \left(\frac{e^{-\lambda_a}\lambda_a^{n-m+1}}{\lambda_a+\xi_k}\right)\left(\frac{e^{-\lambda_a}\lambda_a^{n-m+1}}{\lambda_a+\xi_k}\right)\left(\kappa_{i-1}^{(n-m)}(\lambda_a)^2\,\kappa_{j-1}^{(n-m)}(\lambda_b)^2\right) d\lambda_b d\lambda_a \right.$$
$$\left. - \int_0^{\infty}\int_0^{\infty} \left(\frac{e^{-\lambda_a}\lambda_a^{n-m+1}}{\lambda_a+\xi_k}\right)\left(\frac{e^{-\lambda_b}\lambda_b^{n-m+1}}{\lambda_b+\xi_k}\right)\left(\kappa_{i-1}^{(n-m)}(\lambda_a)\,\kappa_{j-1}^{(n-m)}(\lambda_a)\,\kappa_{i-1}^{(n-m)}(\lambda_b)\,\kappa_{j-1}^{(n-m)}(\lambda_b)\right) d\lambda_b d\lambda_a \right\}. \quad (61)$$

$$\mathbb{E}\left[\mathrm{tr}_{X:Z}\left[\left(\boldsymbol{H}_k\boldsymbol{H}_k^{\mathrm{H}}\right)^{-1}\right]\right] \approx \frac{1}{M_k}\left[3L_k - \frac{3}{M_k}(L_kM_k) + \frac{1}{(M_k)^2}\left[L_k(M_k)^2 + L_k\sum_{k=1}^{K} L_k\mathrm{tr}_{X:Z}\left[\bar{\boldsymbol{R}}\bar{\boldsymbol{R}}_k\right]\right]\right]$$
$$= \frac{1}{(M_k)^3}\left[L_k(M_k)^2 + L_k\sum_{k=1}^{K} L_k\mathrm{tr}_{X:Z}\left[\bar{\boldsymbol{R}}\bar{\boldsymbol{R}}_k\right]\right]. \quad (70)$$

using a known result from matrix differentiation. Invoking the rank-1 adjustment formula [39], we obtain $f_i = -\frac{\partial}{\partial\xi_j}\mathbb{E}\left[\frac{\boldsymbol{X}_i}{1+\boldsymbol{X}_i\theta_i}\right]$, where $\boldsymbol{X}_i = \boldsymbol{v}_i^{\mathrm{H}}\left((\boldsymbol{V}_j)_{:,i}(\boldsymbol{\theta})_{i;i}\left((\boldsymbol{V}_j)_{:,i}\right)^{\mathrm{H}}\right)^{-}\boldsymbol{v}_i$. Now, $\boldsymbol{X}_i$ is exactly the SINR of a minimum-mean-square-error (MMSE) combiner studied in [40]. Denoting $\bar{F}_{X_i}(x_i)$ as the complimentary CDF of $\boldsymbol{X}_i$, $f_i = -\frac{\partial}{\partial\xi_j}\int_0^{\infty}\frac{\bar{F}_{X_i}(x_i)}{1+\theta_i x_i}dx_i$. Since $\bar{F}_{X_i}(x_i)$ is given in [40], f_i can be found by routine integration followed by differentiation w.r.t. ξ_j. Denoting $(\boldsymbol{\theta})_{i;i} = \mathrm{diag}\left[\theta_1^{(i)},\ldots,\theta_{M_j-1}^{(i)}\right]$, we obtain

$$f_i = \frac{\tilde{\tau}_{m_1}\xi_j^{m_1-1}}{(m_1-1)!}I_{i,m_1+1}(\xi_j) - \sum_{l=m_1+1}^{L_j}\frac{\tilde{\tau}_l}{(l-1)!\det(\boldsymbol{\Delta}_0)}$$
$$\times\left((l-1)\xi_j^{l-2}\det(\boldsymbol{\Delta}_1) + \xi_j^{l-1}\det(\boldsymbol{\Delta}_2)\right), \quad (66)$$

where $m_1 = L_j - M_j$, $\tilde{\tau}_l = \begin{cases}1 & \text{if } l\geq 1\\ 0 & \text{otherwise}\end{cases}$ and $I_{i,m_1+1}(\xi_j) = e^{\xi_j/\theta_i}\sum_{s=0}^{m_1-1}\binom{m_1-1}{s}\frac{(-1)^{m_1-1-s}}{\theta_i^{i+1-s}\xi_j^{s-1}}J^{(2)}\left(\frac{\xi_j}{\theta_i}\right)$, respectively. $J^{(2)}\left(\frac{\xi_j}{\theta_i}\right)$ is as defined in (17). Moreover, when $r\neq M_j - L_j + l - 2$, $(\boldsymbol{\Delta}_0)_{r,s} = \left(\theta_s^{(i)}\right)^{r-1}$ and $(\boldsymbol{\Delta}_1)_{r,s} = (\boldsymbol{\Delta}_2)_{r,s} = (\boldsymbol{\Delta}_0)_{r,s}$, whilst when $r = M_j - L_j + l - 2$,

$$(\boldsymbol{\Delta}_1)_{r,s} = \left(\theta_s^{(i)}\right)^r\int_0^{\infty}\frac{x_i^{m_1-1}e^{-\xi_j x_i}}{(1+\theta_i x_i)^2(1+\theta_s^{(i)}x_i)}dx_i \text{ and}$$

$$(\boldsymbol{\Delta}_2)_{r,s} = -\left(\theta_s^{(i)}\right)^r\int_0^{\infty}\frac{x_i^{m_1}e^{-\xi_j x_i}}{(1+\theta_i x_i)^2(1+\theta_s^{(i)}x_i)}dx_i, \quad (67)$$

with both the integrals having closed-form solutions via partial fraction decomposition.

Appendix F
Proof of Theorem 4

From (48), when $N=2$, we have

$$\left(\boldsymbol{H}_k\boldsymbol{H}_k^{\mathrm{H}}\right)^{-1}$$
$$= \frac{1}{M_k}\left[\boldsymbol{I}_{\sum_{i=1}^{K}L_i} - \frac{\boldsymbol{H}_k\boldsymbol{H}_k^{\mathrm{H}}}{M_k} + \boldsymbol{I}_{\sum_{i=1}^{K}L_i} + \frac{1}{(M_k)^2}\right.$$
$$\left.\times\left(\left(\boldsymbol{H}_k\boldsymbol{H}_k^{\mathrm{H}}\right)^2 - 2M_k\boldsymbol{H}_k\boldsymbol{H}_k^{\mathrm{H}} + M_k^2\boldsymbol{I}_{\sum_{i=1}^{K}L_i}\right)\right]$$
$$= \frac{1}{M_k}\left[3\boldsymbol{I}_{\sum_{i=1}^{K}L_i} - \frac{3}{M_k}\boldsymbol{H}_k\boldsymbol{H}_k^{\mathrm{H}} + \frac{1}{(M_k)^2}\left(\boldsymbol{H}_k\boldsymbol{H}_k^{\mathrm{H}}\right)^2\right]. \quad (68)$$

Taking the partial trace of (68) yields

$$\mathrm{tr}_{X:Z}\left[\left(\boldsymbol{H}_k\boldsymbol{H}_k^{\mathrm{H}}\right)^{-1}\right] \approx \frac{1}{M_k}\left[3L_k - \frac{3}{M_k}\mathrm{tr}_{X:Z}\left[\boldsymbol{H}_k\boldsymbol{H}_k^{\mathrm{H}}\right] + \frac{1}{(M_k)^2}\mathrm{tr}_{X:Z}\left[\left(\boldsymbol{H}_k\boldsymbol{H}_k^{\mathrm{H}}\right)^2\right]\right]. \quad (69)$$

After some simplifications, the expected value of (69) can be written as (70), as shown at the top of this page for space reasons. Note that in (70), $\bar{\boldsymbol{R}} \triangleq \frac{\sum_{j=1}^{K}\sum_{l=1}^{L_j}\boldsymbol{R}_{k,l,j}}{\sum_{j=1}^{K}L_j}$ is the average correlation matrix of all terminals and $\bar{\boldsymbol{R}}_k \triangleq \frac{\sum_{l=1}^{L_k}\boldsymbol{R}_{k,l,k}}{L_k}$ is the average correlation matrix for terminals in cell k. Substituting (70) into (47) yields the desired expression in (51).

Acknowledgment

The authors would like to thank Prof. Andreas F. Molisch at University of Southern California, Los Angeles, CA, USA, Prof. Larry J. Greenstein at Rutgers University, North Brunswick, NJ, USA and Dr. Bruno Clerckx at Imperial College London, UK, for the insightful discussions during the course of this work.

REFERENCES

[1] T. L. Marzetta, "Noncooperative cellular wireless with unlimited numbers of base station antennas," *IEEE Trans. Wireless Commun.*, vol. 9, no. 11, pp. 3590–3600, Nov. 2010.

[2] D. Gesbert, M. Kountouris, R. W. Heath, Jr., C.-B. Chae, and T. Sälzer, "Shifting the MIMO paradigm," *IEEE Signal Process. Mag.*, vol. 24, no. 5, pp. 36–46, Sep. 2007.

[3] J. Zhang, R. Chen, J. G. Andrews, A. Ghosh, and R. W. Heath, "Networked MIMO with clustered linear precoding," *IEEE Trans. Wireless Commun.*, vol. 8, no. 4, pp. 1910–1921, Apr. 2009.

[4] C. B. Chae, S. H. Kim, and R. W. Heath, Jr., "Network coordinated beamforming for cell-boundary users: Linear and nonlinear approaches," *IEEE J. Sel. Topics Signal Process.*, vol. 3, no. 6, pp. 1094–1105, Dec. 2009.

[5] D. Gesbert, S. Hanly, H. Huang, S. S. Shitz, O. Simeone, and W. Yu, "Multi-cell MIMO cooperative networks: A new look at interference," *IEEE J. Sel. Areas Commun.*, vol. 28, no. 9, pp. 1380–1408, Dec. 2010.

[6] B. Soret, K. I. Pedersen, N. T. K. Jørgensen, and V. Fernández-López, "Interference coordination for dense wireless networks," *IEEE Commun. Mag.*, vol. 53, no. 1, pp. 102–109, Jan. 2015.

[7] G. Nigam, P. Minero, and M. Haenggi, "Coordinated multipoint joint transmission in heterogeneous networks," *IEEE Trans. Commun.*, vol. 62, no. 11, pp. 4134–4146, Nov. 2014.

[8] H. Tataria, M. Shafi, P. J. Smith, and P. A. Dmochowski, "Coordinated two-tier heterogeneous cellular networks with leakage based beamforming," *CoRR*, pp. 1–6, Mar. 2015.

[9] H. Kim, H. Yu, and Y. H. Lee, "Limited feedback for multicell zero-forcing coordinated beamforming in time-varying channels," *IEEE Trans. Veh. Technol.*, vol. 64, no. 6, pp. 2349–2360, Jun. 2015.

[10] S. Lakshminarayana, M. Assaad, and M. Debbah, "Coordinated multicell beamforming for massive MIMO: A random matrix approach," *IEEE Trans. Inf. Theory*, vol. 61, no. 6, pp. 3387–3412, Jun. 2015.

[11] J. Choi, "Distributed beamforming for macro diversity and power control with large arrays in spatial correlated channels," *IEEE Trans. Wireless Commun.*, vol. 14, no. 4, pp. 1871–1881, Apr. 2015.

[12] C. B. Peel, B. M. Hochwald, and A. L. Swindlehurst, "A vector-perturbation technique for near-capacity multiantenna multiuser communication—Part I: Channel inversion and regularization," *IEEE Trans. Commun.*, vol. 53, no. 1, pp. 195–202, Jan. 2005.

[13] S. Wagner, R. Couillet, M. Debbah, and D. T. M. Slock, "Large system analysis of linear precoding in correlated MISO broadcast channels under limited feedback," *IEEE Trans. Inf. Theory*, vol. 58, no. 7, pp. 4509–4537, Jul. 2012.

[14] H. Tataria, P. J. Smith, P. A. Dmochowski, and M. Shafi, "General analysis of multiuser MIMO systems with regularized zero-forcing precoding under spatially correlated Rayleigh fading channels," in *Proc. IEEE Int. Conf. Commun. (ICC)*, May 2016, pp. 2582–2588.

[15] J. Hoydis, S. ten Brink, and M. Debbah, "Massive MIMO in the UL/DL of cellular networks: How many antennas do we need?" *IEEE J. Sel. Areas Commun.*, vol. 31, no. 2, pp. 160–171, Feb. 2013.

[16] R. Muharar, R. Zakhour, and J. Evans, "Base station cooperation with feedback optimization: A large system analysis," *IEEE Trans. Inf. Theory*, vol. 60, no. 6, pp. 3620–3644, Jun. 2014.

[17] H. S. Dhillon, R. K. Ganti, F. Baccelli, and J. G. Andrews, "Modeling and analysis of K-tier downlink heterogeneous cellular networks," *IEEE J. Sel. Areas Commun.*, vol. 30, no. 3, pp. 550–560, Apr. 2012.

[18] P. J. Smith, C. Neil, M. Shafi, and P. A. Dmochowski, "On the convergence of massive MIMO systems," in *Proc. IEEE Int. Conf. Commun. (ICC)*, Jun. 2014, pp. 5191–5196.

[19] C. Masouros, M. Sellathurai, and T. Ratnarajah, "Large-scale MIMO transmitters in fixed physical spaces: The effect of transmit correlation and mutual coupling," *IEEE Trans. Commun.*, vol. 61, no. 7, pp. 2794–2804, Jul. 2013.

[20] H. Falconet, L. Sanguinetti, A. Kammoun, and M. Debbah, "Asymptotic analysis of downlink MISO systems over Rician fading channels," in *Proc. IEEE Int. Conf. Acoust. Speech Signal Process. (ICASSP)*, May 2016, pp. 3926–3930.

[21] J. Nam, G. Caire, and J. Ha, "On the role of transmit correlation diversity in multiuser MIMO systems," *IEEE Trans. Inf. Theory*, vol. 63, no. 1, pp. 336–354, Jan. 2017.

[22] A. Adhikary, J. Nam, J.-Y. Ahn, and G. Caire, "Joint spatial division and multiplexing—The large-scale array regime," *IEEE Trans. Inf. Theory*, vol. 59, no. 10, pp. 6441–6463, Oct. 2013.

[23] D. Hwang, B. Clerckx, and G. Kim, "Regularized channel inversion with quantized feedback in down-link multiuser channels," *IEEE Trans. Wireless Commun.*, vol. 8, no. 12, pp. 5785–5789, Dec. 2009.

[24] B. Clerckx, G. Kim, and S. Kim, "Correlated fading in broadcast MIMO channels: Curse or blessing?" in *Proc. IEEE Global Commun. Conf. (GLOBECOM)*, Nov./Dec. 2008, pp. 1–5.

[25] P. J. Smith and M. Shafi, "On a Gaussian approximation to the capacity of wireless MIMO systems," in *Proc. IEEE Int. Conf. Commun. (ICC)*, Apr./May 2002, pp. 406–410.

[26] S. L. Loyka, "Channel capacity of MIMO architecture using the exponential correlation matrix," *IEEE Commun. Lett.*, vol. 5, no. 9, pp. 369–371, Sep. 2001.

[27] S. Jin, R. McKay, C. Zhong, and K.-K. Wong, "Ergodic capacity analysis of amplify-and-forward MIMO dual-hop systems," *IEEE Trans. Inf. Theory*, vol. 56, no. 5, pp. 2204–2224, May 2010.

[28] M. Chiani and A. Zanella, "Joint distribution of an arbitrary subset of the ordered eigenvalues of Wishart matrices," in *Proc. IEEE Pers., Indoor Mobile Radio Commun. (PIMRC)*, Sep. 2008, pp. 1–6.

[29] A. Goldsmith, *Wireless Communications*, 2nd ed. Cambridge, U.K.: Cambridge Univ. Press, 2005.

[30] Z. Jiang, A. F. Molisch, G. Caire, and Z. Niu, "Achievable rates of FDD massive MIMO systems with spatial channel correlation," *IEEE Trans. Wireless Commun.*, vol. 14, no. 5, pp. 2868–2882, May 2015.

[31] D. N. Nguyen and T. Le-Ngoc, "MMSE precoding for multiuser MISO downlink transmission with non-homogeneous user SNR conditions," *EURASIP J. Adv. Signal Process.*, vol. 85, no. 1, pp. 1–12, Dec. 2014.

[32] D. A. Basnayaka, P. J. Smith, and P. A. Martin, "Performance analysis of macrodiversity MIMO systems with MMSE and ZF receivers in flat Rayleigh fading," *IEEE Trans. Wireless Commun.*, vol. 12, no. 5, pp. 2240–2251, May 2013.

[33] L. Yu, Y. Liu, and R. Langley, "SINR analysis of the subtraction-based SMI beamformer," *IEEE Trans. Signal Process.*, vol. 58, no. 11, pp. 5926–5932, Nov. 2010.

[34] Q. Zhang, S. Jin, K.-K. Wong, H. Zhu, and M. Matthaiou, "Power scaling of uplink massive MIMO systems with arbitrary-rank channel means," *IEEE J. Sel. Topics Signal Process.*, vol. 8, no. 5, pp. 966–981, Oct. 2014.

[35] O. Lieberman, "A Laplace approximation to the moments of a ratio of quadratic forms," *Biometrika*, vol. 81, no. 4, pp. 681–690, Dec. 1994.

[36] T. M. Cover and J. A. Thomas, *Elements of Information Theory*, 2nd ed. Hoboken, NJ, USA: Wiley, 2005.

[37] D. Zhu, B. Li, and P. Liang, "On the matrix inversion approximation based on Neumann series in massive MIMO systems," in *Proc. IEEE Int. Conf. Commun. (ICC)*, Jun. 2015, pp. 1763–1769.

[38] *Further Advancements for E-UTRA Physical Layer Aspects*, document 3GPP TR 36.814 v.9.0.0, 3GPP, 2010.

[39] R. Horn and C. Johnson, *Matrix Analysis*, 2nd ed. Cambridge, U.K.: Cambridge Univ. Press, 2013.

[40] H. Gao, P. J. Smith, and M. V. Clark, "Theoretical reliability of MMSE linear diversity combining in Rayleigh-fading additive interference channels," *IEEE Trans. Commun.*, vol. 46, no. 5, pp. 666–672, May 1998.

Harsh Tataria (S'13) received the B.E. degree (Hons) in electronic engineering from the Victoria University of Wellington, Wellington, New Zealand, in 2013, and the Ph.D. degree from the Wireless Communications Research Group, Victoria University of Wellington, in 2017. He has recently acquired the Post-Doctoral Research Fellowship with the School of Electronics, Electrical Engineering and Computer Science, Queen's University Belfast, Northern Ireland, U.K. His research interests include statistical analysis of multiple antenna communication systems.

Peter J. Smith (M'93–SM'01–F'15) received the B.Sc. degree in mathematics and the Ph.D. degree in statistics from the University of London, London, U.K., in 1983 and 1988, respectively. From 1983 to 1986, he was with the Telecommunications Laboratories, GEC Hirst Research Center. From 1988 to 2001, he was a Lecturer in statistics with the Victoria University of Wellington, New Zealand. From 2001 to 2015, he was with the Electrical and Computer Engineering Department, University of Canterbury. In 2015, he joined the Victoria University of Wellington as a Professor of Statistics. His research interests include the statistical aspects of design, modeling, and analysis for communication systems, especially antenna arrays, MIMO, cognitive radio, massive MIMO, and mmWave systems.

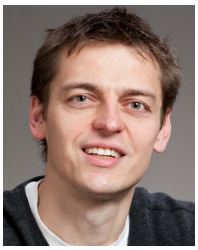

Pawel A. Dmochowski (S'02–M'07–SM'11) was born in Gdańsk, Poland. He received the B.A.Sc. degree in engineering physics from The University of British Columbia in 1998, and the M.Sc. and Ph.D. degrees from Queen's University, Kingston, ON, Canada, in 2001 and 2006, respectively. He was a Natural Sciences and Engineering Research Council Visiting Fellow with the Communications Research Centre Canada. From 2014 to 2015, he was a Visiting Professor with Carleton University, Ottawa. He is currently a Senior Lecturer with the School of Engineering and Computer Science, Victoria University of Wellington, New Zealand. His current research interests include mmWave, massive MIMO, and cognitive radio systems. From 2014 to 2015, he was the Chair of the IEEE Vehicular Technology Society Chapters Committee. He currently serves as an Editor of the IEEE COMMUNICATIONS LETTERS and the IEEE WIRELESS COMMUNICATIONS LETTERS.